Optimization of Co_2MnSi Heusler Alloy Thin Films for Spintronic Applications

By

Yilidaer Abudushalamu

B.S., Tianjin University, 2024

Thesis

Submitted in partial fulfillment of the requirements for the

Degree of Master of Science in the Department of Physics at Brown University

PROVIDENCE, RHODE ISLAND

MAY 2026

This thesis by Yilidaer Abudushalamu is accepted in its present form
by the Department of Physics as satisfying the
thesis requirements for the degree of Master of Science

Date_____ _____

Gang Xiao, Advisor

Signature of Advisor

Approved by the Graduate Council

Date_____ _____

Dean of the Graduate School

Signature of Dean

Acknowledgements

I would first like to express my sincere gratitude to my advisor, Prof. Gang Xiao, for his guidance, support, and encouragement throughout this project. His insight into both physics and experiment, as well as his patience in letting me learn by doing, have shaped the way I think about research.

I am especially indebted to Minh, who taught me in detail how to prepare and process samples in our sputtering system, how to carry out XRD, VSM and other measurements, and who patiently answered countless day-to-day questions in the lab. Many of the practical skills and results in this thesis would not exist without his help and example.

I am also grateful to Benjamin, Liam, and Haoyu for taking the time to explain concepts and techniques that I did not understand at first, and for many helpful discussions about both data and instrumentation. Working with them and the other members of the Xiao group has made the lab a supportive and stimulating environment.

Finally, I would like to thank my family and friends for their continuous encouragement and support during my studies, and for giving me the confidence to pursue this work.

Contents

List of Symbols

d_{hkl}	Interplanar spacing for planes with Miller indices (hkl)
θ	Bragg angle in X-ray diffraction
2θ	Scattering angle in X-ray diffraction
λ	X-ray wavelength
M_{s}	Saturation magnetization
M_{r}	Remanent magnetization
H_{c}	Coercive field
H	Applied magnetic field
R_{P}	Resistance in the parallel magnetic state
R_{AP}	Resistance in the antiparallel magnetic state
R_{s}	Sheet resistance
ρ	Electrical resistivity
R_{q}	Root-mean-square surface roughness
t	Film thickness
T	Temperature
T_{dep}	Deposition temperature
T_{a}	Annealing temperature
E_{F}	Fermi energy
$N(E)$	Electronic density of states as a function of energy

List of Abbreviations

CMS	Co_2MnSi
MTJ	Magnetic tunnel junction
TMR	Tunneling magnetoresistance
DOS	Density of states
FM	Ferromagnetic
XRD	X-ray diffraction
XRR	X-ray reflectivity
XPS	X-ray photoelectron spectroscopy
EDS	Energy-dispersive X-ray spectroscopy
AFM	Atomic force microscopy
VSM	Vibrating sample magnetometry
FMR	Ferromagnetic resonance
SWR	Spin-wave resonance
PPMS	Physical Property Measurement System
PVD	Physical vapor deposition
DC	Direct current
RF	Radio frequency
$L2_1$	Fully ordered full-Heusler structure
B2	Partially ordered CsCl-type structure
A2	Fully disordered bcc-like structure
f.u.	Formula unit

Chapter 1

Introduction

1.1 Motivation: Spintronics and Magnetic Tunnel Junctions

Conventional charge-based electronics has achieved remarkable scaling in density and speed, but further reductions in power consumption and improvements in non-volatility are difficult within purely charge-based device concepts. Spintronics seeks to exploit the electron's spin degree of freedom in addition to its charge, enabling devices in which information is stored and manipulated through the relative orientation of magnetic moments rather than simply through the presence or absence of charge. Magnetic tunnel junctions (MTJs), consisting of two ferromagnetic (FM) electrodes separated by a thin insulating barrier, are a central building block of spintronic technology.

In an MTJ with FM_1/insulator/FM_2 structure, the tunnel resistance depends on the relative orientation of the magnetizations of the two electrodes. When the magnetizations are parallel (P), the resistance is low; when they are antiparallel (AP),

the resistance is higher. The resulting tunneling magnetoresistance (TMR) ratio

$$\mathrm{TMR} = \frac{R_{\mathrm{AP}} - R_{\mathrm{P}}}{R_{\mathrm{P}}} \tag{1.1}$$

is directly related to the spin polarization of the electrodes at the Fermi level. In the ideal limit of two identical half-metallic electrodes with 100% spin polarization and a perfectly symmetric barrier, the TMR can in principle diverge. In practice, the performance of MTJs is limited by finite spin polarization, spin-flip scattering, interface states, and various forms of disorder. Nevertheless, MgO-based MTJs with conventional CoFeB electrodes already achieve large TMR ratios at room temperature, and further improvements require materials with even higher effective spin polarization at interfaces.

Heusler alloys, and in particular Co-based full Heusler compounds, have emerged as leading candidates for highly spin-polarized electrodes in MTJs. In fully epitaxial Co_2MnSi/MgO/Co_2MnSi junctions, giant TMR ratios approaching 2000% at 4.2 K and more than 300% at room temperature have been reported, demonstrating the potential of Co_2MnSi as a nearly half-metallic electrode material when grown and integrated under optimized conditions.[9, 10]

1.2 Heusler Alloys as Half-Metallic Ferromagnets

Heusler alloys form a broad class of intermetallic compounds that can be classified into full Heusler (X_2YZ) and half Heusler (XYZ) families, where X and Y are typically transition metals and Z is a main-group element. Their crystal structures can be described in terms of ordered variants of the cubic $L2_1$, $C1_b$, B2, and A2 structures. In full Heusler compounds with ideal $L2_1$ ordering, the X atoms occupy two interpenetrating fcc sublattices, while Y and Z occupy the remaining two sublattices. Deviations from perfect site ordering, such as B2 (Y/Z disorder) or A2 (complete

disorder), strongly affect their electronic and magnetic properties.[1]

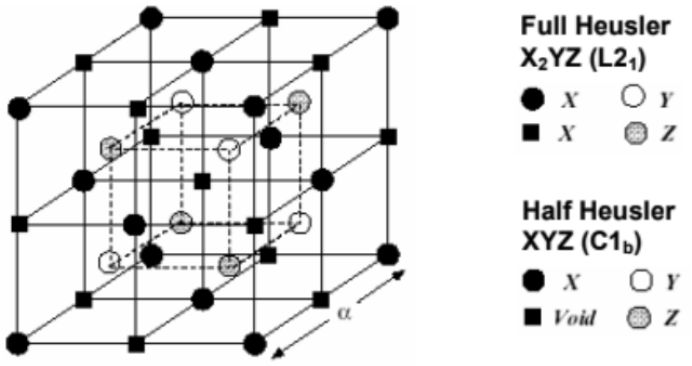

Figure 1.1: Schematic crystal structures of full Heusler (X_2YZ, $L2_1$) and half Heusler (XYZ, $C1_b$) compounds. (adapted from Ref. [2]).

A key attraction of many Heusler alloys is the possibility of half-metallicity: one spin channel is metallic, while the other exhibits a band gap at the Fermi level. In such a half-metal, conduction electrons are fully spin-polarized, making the material an ideal electrode for spin injection and spin filtering. Simple Slater-Pauling rules link the total magnetic moment per formula unit to the number of valence electrons, providing a useful heuristic for identifying candidate half-metallic Heusler compounds.[1] Co-based full Heusler alloys of the form Co_2YZ have been extensively studied because they often combine high Curie temperatures with potentially half-metallic band structures and relatively low resistivities.

Theoretical predictions of half-metallicity in Co_2YZ compounds have motivated numerous experimental studies of their thin-film growth, structural ordering, and magnetic properties.[4, 5, 6, 7, 8, 3] These studies collectively show that achieving half-metallicity in real materials requires careful control of composition, crystalline order, and interfaces.

1.3 Why Focus on Co_2MnSi?

Among Co-based full Heusler alloys, Co_2MnSi (CMS) occupies a special position. It is simultaneously one of the most thoroughly characterized half-metallic candidates and one of the few Heusler compounds to have demonstrated exceptional performance in an actual tunnel junction device. Band structure calculations predict a sizable minority-spin gap and a magnetic moment of $5\,\mu_B$/f.u. consistent with the Slater-Pauling rule,[1] and spin-resolved photoemission has directly confirmed near-complete spin polarization at the Fermi level in epitaxial films.[11] At the device level, fully epitaxial CMS/MgO/CMS junctions have produced TMR ratios exceeding 1000% at low temperature and above 300% at room temperature,[9, 13] placing CMS at the forefront of Heusler-based spintronic materials.

Beyond the performance figures, CMS also has practical advantages that make it well suited to a sputtered MTJ process. Its high Curie temperature of approximately 985 K ensures that ferromagnetic order is stable well above room temperature and under the annealing conditions needed to improve crystalline ordering. Its lattice parameter is closely matched to that of MgO through the standard 45°-rotated epitaxial relationship, making MgO the natural choice for both the substrate template and the tunnel barrier. These properties together make CMS the most logical Heusler electrode material to develop first: the theoretical foundation is strong, the device potential has been experimentally validated, and the material system is compatible with the MgO-based stack architecture that this work is working toward.

1.4 Challenges and Research Gap

Despite the progress achieved in epitaxial CMS films grown on MgO and related single-crystal substrates, realizing CMS-based electrodes with robust and reproducible properties remains challenging, especially when the growth process is implemented

in a practical sputtering system. A central issue is that the ideal Co_2MnSi composition is difficult to preserve during thin-film deposition. Several experimental studies report that sputtered CMS films on Si or Si/SiO_2 can deviate from the ideal 2:1:1 composition, often showing Si-rich and Mn-deficient compositions.[3] Such deviations may arise from differences in sputtering yields among Co, Mn, and Si, preferential oxidation or resputtering of Mn, and possible contributions from the Si substrate, interfacial silicides, or native oxides detected by surface-sensitive techniques such as X-ray photoelectron spectroscopy (XPS). Since the half-metallic electronic structure is sensitive to antisite disorder and off-stoichiometry, even a film that appears structurally recognizable as CMS may have a reduced magnetic moment and a lower effective spin polarization.

Composition control is closely connected to crystalline ordering. The half-metallic band structure of Co_2MnSi is associated with the ordered $L2_1$ full-Heusler structure, but this ordering is not automatically obtained in sputtered films. In polycrystalline films grown on amorphous or poorly lattice-matched substrates, partial B2 order, A2-like disorder, and antisite defects can coexist with the main CMS phase. FMR and spin-wave resonance measurements on CMS films with different degrees of crystalline order show that magnetic anisotropy, exchange stiffness, and damping are all sensitive to structural order and defect density.[8, 6] This means that XRD peak formation alone is not enough; the growth process must also be evaluated through magnetic and transport measurements.

For MTJ applications, the problem extends beyond the CMS film itself. Most of the highest TMR values reported for CMS-based MTJs use epitaxial $Co_2MnSi/MgO/Co_2MnSi$ stacks on single-crystal substrates and rely on carefully optimized annealing to improve $L2_1$ order and reduce interface disorder.[13, 9, 10] In these structures, MgO is not simply an insulating spacer. It acts as a crystalline tunnel barrier whose symmetry filtering effect depends strongly on the quality of the adjacent ferromag-

net/barrier interfaces. A CMS film that is ferromagnetic and metallic on Si/SiO_2 may therefore still be far from a useful MTJ electrode if the surface is too rough, if the MgO barrier cannot be grown uniformly, or if minority-spin interface states dominate the tunneling process.

These considerations define the practical gap addressed in this thesis. The work begins with the problem of composition control, first through an exploratory composite Co/Mn/Si target and then through a commercial CMS bulk target on Si/SiO_2. The Si/SiO_2 samples provide a convenient baseline for correlating composition, XRD structure, magnetization, and resistivity. The project then moves to MgO substrates and MgO buffer layers, where the emphasis shifts from simply obtaining ferromagnetic CMS films to preparing a smooth and device-relevant CMS/MgO interface. In this way, the thesis follows the materials path required for future CMS/MgO/CMS MTJ fabrication rather than treating thin-film growth and device design as separate problems.

1.5 Objectives and Structure of the Thesis

The primary goal of this thesis is to develop sputtered Co_2MnSi thin films and MgO-based heterostructures as a materials foundation for future CMS/MgO/CMS magnetic tunnel junctions. The work is motivated by the gap between the ideal properties predicted for Co_2MnSi and the practical requirements of an actual MTJ stack. In a device-relevant structure, it is not sufficient for CMS to be merely ferromagnetic; its composition, crystalline order, surface morphology, and interface with MgO must all be controlled well enough to support spin-dependent tunneling.

The project therefore follows the experimental path by which the material system was developed in the laboratory. Before the commercial CMS alloy target became available, a composite Co/Mn/Si target was explored as an early route to composi-

tion control. This stage tested whether the relative elemental fluxes could be tuned through target geometry, and it also revealed the practical difficulty of maintaining the desired Co:Mn:Si ratio during sputtering. After the CMS bulk target arrived, the focus shifted to films grown on Si/SiO_2 substrates. These samples provided a reproducible baseline for evaluating CMS growth by XPS, XRD, VSM, and four-probe resistivity measurements. Although Si/SiO_2 is not the ideal template for high-TMR epitaxial junctions, it is a useful platform for establishing whether the sputtering process can produce crystalline, ferromagnetic, and metallic CMS films.

The later part of the work moves from this baseline film study toward MgO-based heterostructures. Since MgO is central to the highest-performance CMS/MgO/CMS MTJs reported in the literature, MgO substrates and MgO buffer layers were introduced to provide a more relevant template for future device stacks. AFM measurements were used to monitor the roughness evolution after substrate annealing, MgO buffer deposition, and CMS growth. This part of the project connects the magnetic film optimization to the interface requirements of an MTJ, where the MgO tunnel barrier will eventually be only a few nanometers thick.

The thesis also includes preliminary preparation for CMS/MgO/CMS device fabrication. MgO barrier growth was calibrated by X-ray reflectivity and MTJ masks were designed for future transport measurements. The intended device concept is to use two CMS electrodes with different thicknesses so that their different coercive fields allow parallel and antiparallel magnetic states to be selected during a field sweep, enabling measurement of the tunneling magnetoresistance.

The remainder of this thesis is organized as follows. Chapter 2 reviews the crystal structure, electronic properties, and MTJ performance of Co_2MnSi and related Heusler alloys. Chapter 3 introduces the sputtering, structural, magnetic, surface, and transport characterization techniques used in this work. Chapter 4 describes the experimental procedures, including the composite target exploration, CMS growth on

Si/SiO_2, MgO substrate and buffer preparation, and CMS growth on MgO. Chapter 5 presents the experimental results following this step-by-step development route, from composition control and baseline film growth to MgO-based interface optimization. Chapter 6 discusses the proposed CMS/MgO/CMS MTJ architecture, the switching strategy based on coercive field asymmetry, the fabrication sequence and mask design, the remaining materials gaps between the current films and the requirements for high TMR, and the priority directions for future optimization and device fabrication. Chapter 7 summarizes the main findings and contributions of this work.

Chapter 2

Heusler Alloys and Co_2MnSi: Structure and Electronic Properties

2.1 Crystal Structures of Heusler Alloys

Heusler compounds are ternary intermetallics with compositions of the form X_2YZ (full Heusler) or XYZ (half Heusler), where X and Y are typically transition metals and Z is a main-group element. Half Heusler compounds adopt the $C1_b$ structure (space group $F\bar{4}3m$), which can be viewed as a zincblende lattice in which one of the four fcc sublattices is vacant. Full Heusler compounds with ideal $L2_1$ ordering (space group $Fm\bar{3}m$) fill all four sublattices: the X atoms occupy the $8c$ and $4a$ sites, while Y and Z occupy the $4b$ and $4d$ sites, respectively. The resulting long-range chemical order gives rise to characteristic superlattice reflections in XRD patterns. The crystal structures of both families are illustrated in Fig. 2.1.

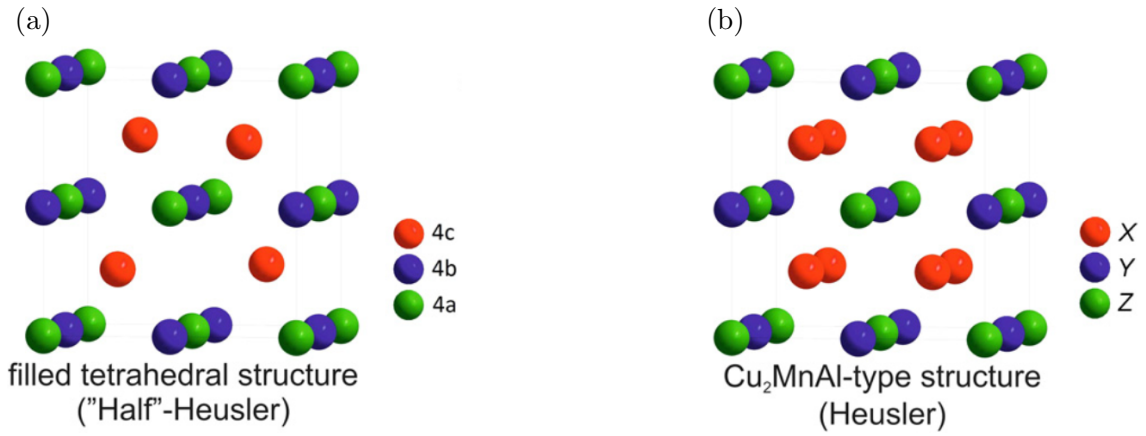

Figure 2.1: Crystal structures of (a) half-Heusler XYZ ($C1_b$) and (b) full Heusler X_2YZ ($L2_1$) compounds (adapted from Ref. [1]).

In practice, full Heusler films rarely achieve perfect $L2_1$ order, and several types of site disorder are commonly observed.[1] In the B2 structure (CsCl-type, space group $Pm\bar{3}m$), the Y and Z atoms are randomly distributed over their two sublattices while the X sublattices remain ordered. In the fully disordered A2 case, all three elements are randomly distributed over a single bcc lattice. These ordering states can be distinguished by XRD: the (111) superlattice reflection appears only in $L2_1$, the (200) reflection is present in both $L2_1$ and B2 but absent in A2, while the fundamental (220) and (400) reflections appear regardless of ordering state.[5, 6] Figure 2.2 illustrates this distinction for a Co_2Mn-based Heusler alloy.

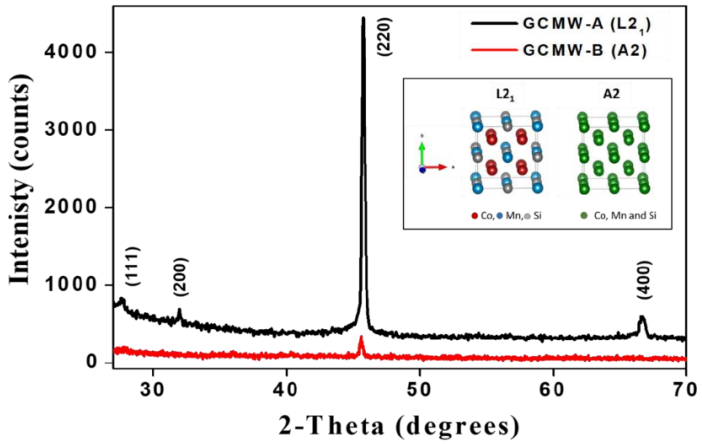

Figure 2.2: XRD patterns of a Co_2Mn-based Heusler alloy in the $L2_1$ and A2 ordering states. Superlattice reflections (111) and (200) are present only in $L2_1$ (adapted from Ref. [16]).

2.2 Half-Metallicity and Co_2MnSi

A key attraction of many Heusler alloys is the possibility of half-metallicity: one spin channel is metallic while the other exhibits a band gap at the Fermi level, leading to fully spin-polarized conduction electrons. For full Heusler alloys X_2YZ, the electronic structure arises from strong hybridization between the d states of the transition metals and the p states of the main-group element. In Co-based full Heuslers, the majority-spin bands are metallic and cross the Fermi level, while the minority-spin bands develop a gap due to hybridization and crystal-field splitting in the $L2_1$ structure.[1] The resulting spin-resolved DOS is shown schematically in Fig. 2.3.

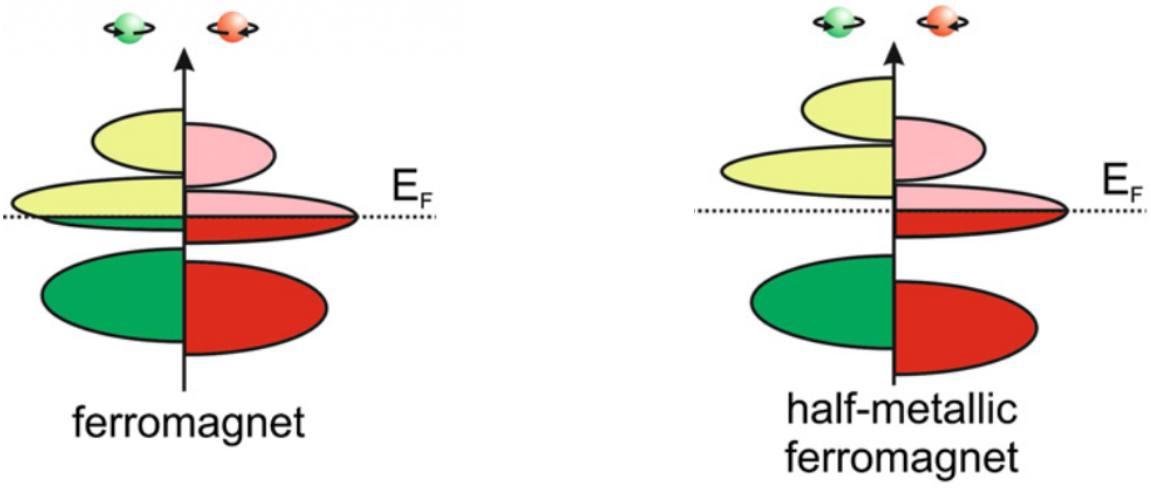

Figure 2.3: Schematic spin-resolved densities of states for a ferromagnet and a half-metallic ferromagnet (adapted from Graf *et al.*[1]).

A simple rule connecting electronic structure to magnetic properties is provided by the Slater-Pauling relation. For full Heuslers, the total spin moment per formula unit m (in μ_B/f.u.) is often close to

$$m \approx N_V - 24,$$

where N_V is the total number of valence electrons.[1] When the Fermi level lies in the minority gap, changes in N_V are accommodated entirely by majority-spin electrons,

giving a linear dependence of m on N_{V}. Deviations from this line signal departures from perfect half-metallicity due to disorder or off-stoichiometry.

Within the Co_2YZ family, compounds such as Co_2MnGe, Co_2MnSn, and Co_2FeSi have all been explored as spintronic electrodes.[1] Co_2MnSi stands out among these for three reasons. Its predicted minority-spin gap of 0.4–0.8 eV is among the largest in the family, its Curie temperature of approximately 985 K ensures ferromagnetic stability well above room temperature, and its lattice parameter is closely matched to MgO through the standard 45°-rotated epitaxial relationship, making MgO the natural choice for both the substrate and the tunnel barrier.[1, 5] For a 29-valence-electron system, the Slater-Pauling rule predicts a moment of $5\,\mu_{\mathrm{B}}$/f.u., consistent with the half-metallic ground state.

Experimental work confirms that high-quality CMS films can approach this ideal. Pandey *et al.* reported a moment of $4.95\,\mu_{\mathrm{B}}$/f.u. and an $L2_1$ ordering parameter of about 96% in epitaxial films annealed at 600°C, with exchange stiffness and magnetic anisotropy evolving systematically with crystalline order.[8] Most directly, Jourdan *et al.* measured a spin polarization of $(93^{+7}_{-11})\%$ at the Fermi level using spin-resolved photoemission, providing direct spectroscopic confirmation of the predicted minority-spin gap.[11] Transport measurements on epitaxial CMS films show metallic resistivity and negative magnetoresistance at low temperatures, consistent with a highly spin-polarized ferromagnet.[12]

2.3 Disorder, Composition, and Their Consequences

The half-metallic properties of Co_2MnSi depend critically on achieving the correct crystal structure and composition. The most detrimental form of disorder is the Co-Mn antisite, in which Co and Mn exchange lattice positions, introducing localized states in the minority-spin gap and directly suppressing spin polarization.[1] More

broadly, partial B2 or A2 disorder reduces the long-range chemical order that the half-metallic band structure requires. Pandey *et al.* showed that increasing $L2_1$ order through higher annealing temperatures raises M_s and sharpens FMR spectra, while Belmeguenai *et al.* found that structural and magnetic properties evolve together across a range of growth conditions.[8, 6]

Composition control is equally important. Ishikawa *et al.* systematically varied the Mn content in $Co_2Mn_\alpha Si$ electrodes and found that Mn-rich compositions ($\alpha > 1$) suppress Co-Mn antisites, reduce minority-spin gap states, and yield substantially higher TMR than nearly stoichiometric films.[14] This result establishes that the target for CMS electrode growth is not simply the nominal 2:1:1 stoichiometry, but a slightly Mn-rich composition that minimizes antisite disorder. As will be shown in Chapter 5, the sputtered CMS films in this work consistently show Mn deficiency, placing them on the wrong side of this composition dependence and motivating the composition engineering strategies discussed in Chapter 6.

2.4 Co_2MnSi-Based MTJs in the Literature

The strongest motivation for using Co_2MnSi as a spintronic electrode comes from CMS/MgO/CMS magnetic tunnel junctions. Ishikawa *et al.* fabricated fully epitaxial Co_2MnSi/MgO/Co_2MnSi MTJs on MgO(001) substrates and reported TMR ratios of about 683% at 4.2 K and 179% at room temperature.[13] MgO-thickness-dependent TMR oscillations confirmed that coherent tunneling through the crystalline MgO barrier plays an important role, establishing CMS/MgO/CMS as one of the most promising Heusler-based MTJ systems.

Further optimization showed that the structural template and buffer layers can strongly influence MTJ performance. Liu *et al.* introduced a CoFe-buffered MgO(001) substrate and reported TMR ratios up to 1995% at 4.2 K and 354% at 290 K, among

the largest values reported for any Heusler-based MTJ.[9] The enhancement was attributed to the combination of high intrinsic spin polarization in CMS and coherent Δ_1 tunneling through MgO.

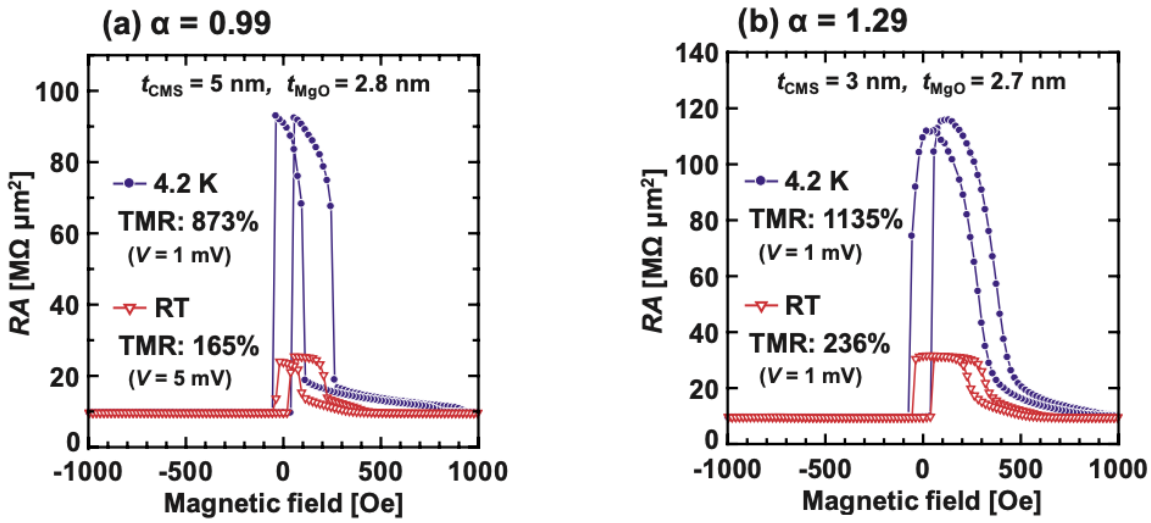

Figure 2.4: TMR curves for CMS/MgO/CMS MTJs with (a) nearly stoichiometric (α = 0.99) and (b) Mn-rich ($\alpha = 1.29$) CMS electrodes (adapted from Ref. [14]).

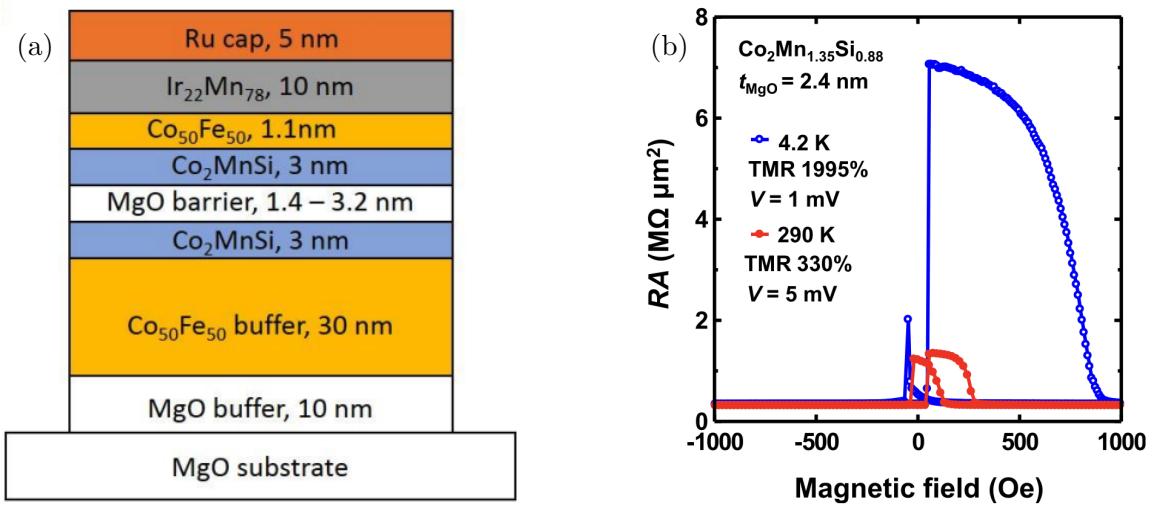

Figure 2.5: (a) CoFe-buffered CMS/MgO/CMS stack and (b) giant TMR in an optimized epitaxial CMS/MgO/CMS MTJ (adapted from Liu *et al.* [9] and Hu *et al.*[15]).

Tunneling spectroscopy studies revealed that the CMS/MgO interface is a critical limiting factor. Ishikawa *et al.* showed from dI/dV analysis that minority-spin interface states near the Fermi level strongly suppress the effective spin polarization in

tunneling, even when the bulk electrodes are close to half-metallic.[10] These results show why simply obtaining ferromagnetic CMS films is not sufficient: the composition, crystalline ordering, and interface quality must all be controlled together to realize large TMR. This is the materials challenge that the present thesis works toward, beginning with the establishment of a sputtered CMS baseline and progressing toward MgO-based heterostructure preparation for future CMS/MgO/CMS junctions.

Chapter 3

Magnetron Sputtering and Characterization Techniques

3.1 Principles of Magnetron Sputtering

Magnetron sputtering is a widely used physical vapour deposition (PVD) technique for growing metallic and compound thin films with good uniformity and thickness control.[17] In a DC magnetron configuration, a negative voltage is applied to the target, which serves as the cathode, while the chamber walls and the substrate holder are near ground potential. After evacuating the chamber to high vacuum, an inert sputter gas, typically argon, is introduced to a working pressure in the 10^{-3}–10^{-2} Torr range. When the applied voltage exceeds the breakdown field of the gas, a glow discharge is ignited and a quasi-steady-state plasma forms in front of the target.

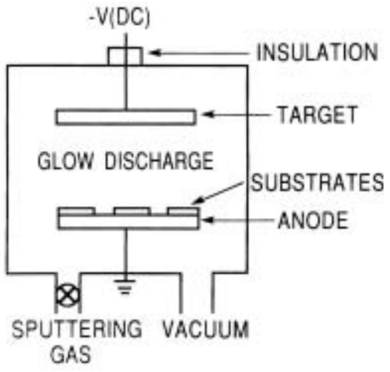

Figure 3.1: Schematic diagram of a DC sputtering system (adapted from Ref. [2]).

Positive Ar^+ ions in the plasma are accelerated towards the negatively biased target and bombard its surface. The energy transferred from the incident ions to target atoms through a cascade of collision events can eject target atoms, a process quantified by the sputter yield Y, defined as the number of sputtered atoms per incident ion.[18] In Sigmund's linear cascade theory, Y scales approximately with the ratio of ion energy to target surface binding energy, modulated by the efficiency of momentum transfer, and depends on both ion species and target composition.[18] Besides sputtered target atoms, the ion bombardment also generates secondary electrons, reflected neutrals, and occasionally implanted ions. The sputtered atoms leave the surface with typical kinetic energies of a few to a few tens of eV and undergo collisions with the background gas on their way to the substrate, so that sputtering is not a purely line-of-sight process.[17]

The distinctive feature of magnetron sputtering is the use of a magnetic field behind the target to confine electrons close to its surface. In a planar magnetron, permanent magnets are arranged so that the magnetic field lines emerge from the target in one region, run parallel to the surface, and return to the target elsewhere. Electrons emitted from the cathode then experience crossed electric and magnetic fields and undergo cycloidal $E \times B$ drift orbits near the target, which greatly increases the probability of ionizing collisions with Ar atoms.[17] As a result, the plasma is

localized in a toroidal "racetrack" region above the target, the ion current is enhanced, and the discharge can be sustained at much lower gas pressures than in simple diode sputtering. The higher ion flux yields significantly higher deposition rates, often approaching an order of magnitude above those of conventional dc sputtering, while the reduced pressure increases the mean free path of sputtered atoms and can improve film density and mitigate scattering-induced compositional shifts.

Film growth during magnetron sputtering is controlled by a combination of kinetic and thermodynamic factors. The working gas pressure, discharge power, target-to-substrate distance, and substrate temperature all influence the adatom flux, energy, and mobility at the growing interface.[17, 2] At low substrate temperatures and relatively high gas pressures, adatom mobility is limited and the film tends to develop a porous, fine-grained columnar morphology, often described by Thornton's zone model.[19] Increasing the substrate temperature or lowering the pressure promotes surface diffusion, leading to denser films with larger grains and, for suitable substrates and lattice mismatch, even epitaxial growth. In addition, energetic particle bombardment can induce resputtering, intermixing, and defect formation, which are particularly relevant for multicomponent alloys such as Heusler compounds.

In this thesis, RF sputtering was used for the main CMS bulk-target series and for MgO deposition, while the general sputtering physics described above applies to both metallic and insulating targets with appropriate power supply configuration. For metallic CMS, RF sputtering provided stable plasma conditions in the available system, and for insulating MgO it was necessary to sustain the discharge without charge buildup on the target surface.

3.2 Composite-Target and Alloy-Target Sputtering for CMS Growth

For multicomponent alloys such as Co_2MnSi, controlling the film stoichiometry is a central challenge. Ideally, the arriving Co, Mn, and Si fluxes should produce the full-Heusler composition Co:Mn:Si = 2:1:1. In practice, however, the deposited composition can differ from the nominal target composition because the sputtering yields, angular distributions, oxidation tendencies, and resputtering rates of the constituent elements are not the same.

Two source strategies were considered in this work. The first was an exploratory composite target assembled from separate Co, Mn, and Si pieces. In a simple area-weighted picture, the time-averaged flux Φ_i of element i arriving at the substrate may be approximated as

$$\Phi_i \propto f_i Y_i I_{\mathrm{ion}},$$

where f_i is the fractional target area occupied by element i, Y_i is its sputtering yield under the chosen plasma conditions, and I_{ion} is the ion current to the target. This expression is useful as a first guideline, but it is only approximate. In a real magnetron, the erosion racetrack is nonuniform, the local plasma density varies across the target, and different elements may have different angular emission distributions. Therefore, the film composition cannot be determined from target area alone.

The second strategy was to use a commercial Co_2MnSi alloy target. This route is more reproducible because the target already contains Co, Mn, and Si in a nominal Heusler composition. However, even an alloy target does not guarantee a stoichiometric film. Preferential sputtering, Mn oxidation, and interfacial contributions from the substrate can still cause the measured film composition to deviate from the ideal 2:1:1 ratio. Both strategies were explored in this work and are described in detail in Chapter 4; their compositional outcomes are discussed in Chapter 5.

3.3 Structural Characterization

X-ray diffraction (XRD) is the primary tool used in this work to assess the crystal structure, texture, and degree of ordering in Co_2MnSi thin films. In a standard θ-2θ scan, the incident angle θ of the X-ray beam with respect to the sample surface and the detector angle 2θ are varied in a coupled fashion, so that only lattice planes parallel to the substrate surface contribute to the diffraction condition. The positions of the diffraction peaks follow Bragg's law $2d_{hkl}\sin\theta = n\lambda$, where d_{hkl} is the spacing of the lattice planes with Miller indices (hkl) and λ is the X-ray wavelength.[20]

For full Heusler alloys with the $L2_1$ structure, such as Co_2MnSi, the presence or absence of certain fundamental and superlattice reflections provides information about long-range chemical order.[1] The (220) and (400) reflections are fundamental fcc-type peaks that appear regardless of whether the Y and Z atoms are ordered or disordered; they thus serve to determine the basic lattice parameter and assess overall crystallinity. In contrast, the (111) reflection is sensitive to the ordering between Y and Z, appearing only in the fully ordered $L2_1$ structure and vanishing in the B2 or A2 disordered states. The (200) reflection is present in both $L2_1$ and B2 structures but disappears in the fully disordered A2 phase.[1, 5] By comparing the relative intensities of these peaks to calculated structure factors or to reference data, a qualitative ordering parameter can be estimated.[6]

In polycrystalline Co_2MnSi films grown on amorphous or poorly lattice-matched substrates such as Si/SiO_2, the diffraction patterns typically show strong (220) texture with weaker higher-order peaks, reflecting growth along close-packed directions.[5, 3] The full width at half maximum (FWHM) of the peaks provides information about crystallite size and microstrain via the Scherrer formula and Williamson–Hall analysis, although instrumental broadening and texture effects must be considered.[20] When necessary, X-ray reflectivity (XRR) measurements at very small incident angles can be used to determine total film thickness and interface roughness from Kiessig fringes,

complementing profilometry or cross-sectional electron microscopy.[17]

3.4 Magnetic Characterization

The magnetic properties of Co_2MnSi films in this thesis are characterized primarily by vibrating sample magnetometry (VSM), with supplementary magnetotransport measurements carried out in a Physical Property Measurement System (PPMS) where appropriate. In a VSM, the sample is placed in a uniform dc magnetic field and mechanically oscillated, typically at a frequency of a few tens of Hz, perpendicular to the field direction.[21] The changing magnetic flux through a set of pickup coils induces a voltage proportional to the time derivative of the sample magnetic moment; phase-sensitive detection at the drive frequency yields a signal proportional to the magnetization. By sweeping the applied field and recording the induced voltage, one obtains hysteresis loops $M(H)$ from which key parameters such as saturation magnetization M_s, remanence M_r, and coercive field H_c are extracted.

Thin-film samples are typically measured with the magnetic field applied in the plane of the film to minimize demagnetizing effects.[21, 2] The in-plane $M(H)$ loops of Co_2MnSi films often show relatively square hysteresis with modest coercivity when the films are well crystallized and have strong texture along a particular easy axis.[6, 8] Deviations from the bulk saturation magnetization can indicate incomplete $L2_1$ ordering, off-stoichiometry, or the presence of magnetically dead layers near interfaces. In addition, measurements as a function of temperature can be used to estimate the Curie temperature or to identify spin reorientation phenomena, although in Co_2MnSi the Curie temperature is well above room temperature.

Ferromagnetic resonance (FMR) and spin-wave resonance (SWR) measurements, while not the primary focus here, provide complementary information on dynamic magnetic properties such as the effective anisotropy fields, exchange stiffness, and

damping.[8] In Co_2MnSi films, these quantities are sensitive to crystalline order and can thus serve as additional probes of structural quality. For device-relevant structures, low-temperature magnetotransport measurements in a PPMS allow the determination of anisotropic magnetoresistance, Hall effects, and TMR.

3.5 Compositional and Surface Characterization

Accurate determination of the Co:Mn:Si ratio and the chemical state of each element is crucial for understanding and optimizing Co_2MnSi thin films. In this work, composition and surface chemistry were probed mainly by X-ray photoelectron spectroscopy (XPS) and energy-dispersive X-ray spectroscopy (EDS), while surface morphology and roughness were characterized by atomic force microscopy (AFM). These techniques provide complementary information: XPS is sensitive to the near-surface chemical composition, EDS gives a more averaged composition over a larger interaction volume, and AFM directly probes the topographic morphology of the film surface.

XPS is a surface-sensitive technique in which core-level electrons are excited by monochromatic X-rays and their kinetic energies are analyzed to yield binding-energy spectra characteristic of the elements present and their chemical environment.[22] For commonly used Al Kα or Mg Kα sources, the inelastic mean free path of photoelectrons in metals is on the order of 1–3 nm, so that XPS probes only the top few nanometers of the film. Peak positions and line shapes in the Co $2p$, Mn $2p$, and Si $2p$ regions can be used to distinguish metallic species from oxidized species and to identify chemical shifts associated with surface oxidation or interfacial compounds.[22] Quantitative composition estimates are obtained by integrating peak areas and applying relative sensitivity factors, although corrections for background, overlapping peaks, preferential sputtering, and instrumental broadening may be required.

For Co_2MnSi films on Si/SiO_2, XPS composition values must be interpreted with particular care. Because the measurement is surface sensitive, the detected Si signal may include contributions from surface oxidation, interfacial SiO_2, or substrate-related signals, depending on the film thickness and measurement condition. Therefore, in this thesis, XPS is used primarily to identify compositional trends, such as Mn deficiency and apparent Si enrichment, rather than as an absolute measure of the bulk CMS stoichiometry.

EDS, by contrast, detects characteristic X-ray emission induced by an electron beam in a scanning electron microscope.[23] The electron interaction volume in SEM-based EDS typically extends from hundreds of nanometers to several micrometers into the sample, depending on the accelerating voltage and material density. As a result, EDS gives a more bulk-averaged composition than XPS, but in thin-film-on-substrate geometries it can also be strongly influenced by the substrate unless low beam energies or cross-sectional geometries are used.[23, 2] In this work, EDS was used mainly to evaluate relative composition trends and to compare the elemental balance associated with different target designs.

Surface roughness was characterized by AFM, especially for MgO substrates, MgO buffer layers, and CMS films grown on MgO. This measurement is important for MTJ development because the MgO tunnel barrier is expected to be only a few nanometers thick. Roughness in the substrate, buffer layer, or bottom magnetic electrode can lead to nonuniform barrier thickness, local current crowding, pinholes, and degraded tunneling magnetoresistance. AFM provides a direct height map of the surface by scanning a sharp tip across the sample and recording the tip-surface interaction.

The root-mean-square roughness R_q was used as the main quantitative measure of surface morphology:

$$R_q = \sqrt{\frac{1}{N}\sum_{i=1}^{N}(z_i - \bar{z})^2},$$

where z_i is the height at the i-th pixel, $\bar{z}$ is the average height, and N is the total number of pixels in the scanned area. For MgO-based samples, AFM was performed after substrate annealing, MgO buffer deposition, and CMS growth to monitor how each processing step affected the surface. When necessary, image flattening or background subtraction was used to remove large-scale sample tilt or scanner curvature before comparing RMS roughness values.

3.6 Electrical Transport Characterization

Room-temperature electrical resistivity was measured using a four-probe configuration. This method is preferred over a two-probe measurement because the current is applied through the outer probes while the voltage is measured between the inner probes, reducing the influence of contact resistance and lead resistance. For conducting thin films such as Co_2MnSi, this is important because the intrinsic film resistance can be comparable to or smaller than parasitic contact contributions.

For a thin film, the resistivity can be calculated from the sheet resistance R_s and film thickness t:

$$\rho = R_s t.$$

For a rectangular measurement geometry, the same relationship can be written as

$$\rho = R\frac{wt}{L},$$

where R is the measured resistance, w is the width of the conducting path, t is the film thickness, and L is the distance between the voltage probes. In this thesis, four-probe measurements were used to determine whether CMS films grown on Si/SiO_2 exhibit metallic transport and whether their resistivity values are reasonable for use as conducting electrodes in future MTJ structures.

Chapter 4

Experimental Methods

4.1 Deposition System and Substrates

All Co_2MnSi thin films in this work were deposited in a high-vacuum magnetron sputtering system in our laboratory. The system is designed for the fabrication of single-layer and multilayer structures from metals, insulators, and semiconductors. It is equipped with six 2-inch magnetron sputtering guns mounted in a confocal geometry, one substrate heater, and a plasma oxidation source. Both DC and RF power supplies are available, allowing metallic as well as insulating targets to be sputtered under appropriate conditions. Fast shutters, feedback control of gas pressure, and substrate temperature make it possible to reproducibly grow nanoscale multilayers on wafers up to 2 inch in diameter.[17, 2]

Before each growth, the main chamber was pumped down to a base pressure typically in the low 10^{-7} Torr range. A low base pressure is important for minimizing residual oxygen and water, which can oxidize reactive elements such as Mn during deposition.[3, 7] Argon was used as the sputtering gas for both Co_2MnSi and MgO deposition. For the main CMS bulk-target series and for CMS deposition on MgO-based templates, the Ar working pressure was approximately 2.03 mTorr. For MgO

buffer deposition, a lower Ar pressure of approximately 1.4 mTorr was used.

The first part of this work used 2-inch Si(100) wafers with a thermally grown SiO_2 layer. The amorphous SiO_2 layer suppresses direct silicide formation and interdiffusion, but precludes epitaxial growth and instead promotes textured polycrystalline films.[5, 3] In the later part of the project, the growth route was transferred to MgO(001) substrates, motivated by the CMS/MgO/CMS MTJ literature where MgO substrates, buffer layers, and tunnel barriers are used to promote crystalline growth and coherent tunneling.

4.2 Characterization Workflow

The characterization workflow was designed to connect each experimental stage with the specific materials question it was intended to answer. For the composite-target work, the central question was whether a segmented Co/Mn/Si target could produce a film composition close to the ideal Co_2MnSi ratio. EDS was used as a rapid composition check after film deposition, and the target geometry was adjusted according to the measured Co, Mn, and Si balance. XPS was then used to obtain a more detailed near-surface composition analysis.[22, 23]

For the CMS films grown from the commercial bulk target on Si/SiO_2, the goal was to establish a baseline process and correlate composition, structure, magnetism, and transport. XPS was used to evaluate near-surface composition and check for Mn deficiency. XRD was used to identify CMS-related crystalline reflections and look for evidence of partial chemical ordering.[20] VSM measurements determined the saturation magnetization, coercive field, and hysteresis-loop shape, with angle-dependent VSM used on selected samples to identify in-plane easy and hard axes.[21] Four-probe measurements confirmed metallic transport in the films.

For the MgO-based part of the project, the characterization emphasis shifted

toward interface preparation. AFM was used after each processing step to monitor surface roughness evolution, which is especially critical because the future MgO tunnel barrier will be only a few nanometers thick. XRR was used to evaluate film thickness and interface quality, and to calibrate the MgO deposition rate for future tunnel-barrier growth.[17] VSM was used to compare the magnetization and anisotropy of CMS-on-MgO films with the Si/SiO_2 baseline. XRD characterization of the MgO-based CMS films is currently in progress.

More advanced techniques such as ferromagnetic resonance, transmission electron microscopy, and tunneling spectroscopy have been used in other Co_2MnSi studies[8, 13, 10, 9] but lie beyond the experimental scope of this thesis.

4.3 Composite Target Design and Early Composition Exploration

Before the commercial Co_2MnSi alloy target became available, a composite Co/Mn/Si target was designed and fabricated as an early route for exploring CMS growth. In this design, the 2-inch cathode face was populated with separate Co, Mn, and Si pieces so that the relative Co:Mn:Si flux could be partly adjusted through the geometry of the target surface rather than being fixed by the stoichiometry of a single alloy target.[2, 7]

The target layout was designed with Co sectors, Mn fan-shaped regions, and Si insert regions distributed across the sputtering surface, as shown in Fig. 4.1. Co, Mn, and Si pieces were cut from high-purity plates by wire electrical discharge machining (EDM), polished to remove burrs, and mechanically clamped to the water-cooled copper backing plate.

Because a planar magnetron erodes the target mainly within a racetrack rather than uniformly, the visible areas of the Co, Mn, and Si pieces cannot be directly con-

verted into the final film composition. The deposited composition also depends on the sputtering yield, angular distribution, and oxidation tendency of each element.[2, 7] The initial design was therefore evaluated by depositing test films and measuring their composition by EDS, which showed clear deviation from the desired stoichiometry. Guided by these results, the relative exposed areas of the Mn, Co, and Si pieces were adjusted, as shown in Fig. 4.1(c). After this adjustment, XPS analysis still showed Mn deficiency and Si enrichment relative to the ideal Co:Mn:Si = 2:1:1 ratio, indicating that simple geometric control of target area was insufficient to produce stoichiometric CMS. This result motivated the transition to the commercial CMS bulk target.

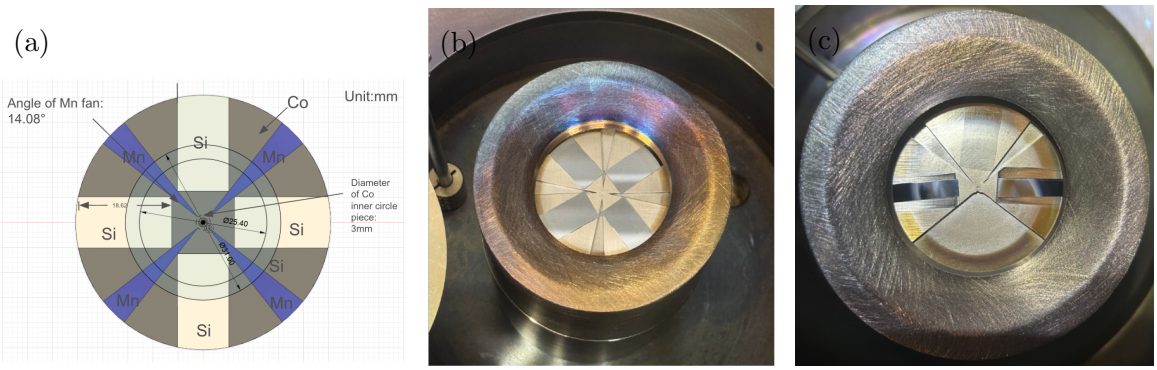

Figure 4.1: Composite Co/Mn/Si sputtering target. (a) Conceptual design. (b) Initial implementation. (c) Optimized geometry after adjusting Mn and Si sector sizes.

4.4 CMS Thin-Film Growth on Si/SiO_2

After the composite-target exploration, the commercial Co_2MnSi bulk target was used as the main route for systematic CMS film growth. The target was a 2-inch diameter, 3-mm thick Co_2MnSi disk with a nominal Co:Mn:Si composition of 2:1:1.[2, 8] It was clamped to a water-cooled copper backing plate and pre-sputtered for several minutes before each deposition to remove surface contamination and reach steady-state operating conditions.

RF sputtering at 60 W and an Ar working pressure of approximately 2.03 mTorr were used for the main bulk-target temperature series. The representative samples

were MNC059, MNC053/MNC056, MNC057, and MNC060, corresponding to deposition temperatures of 480, 500, 520, and 540°C, respectively. The deposition rate was calibrated by XRR, and film thickness was controlled by adjusting the sputtering duration.

Post-deposition annealing is important for promoting $L2_1$ ordering and improving the magnetic properties of Co_2MnSi.[6, 8] In this work, the systematic comparison focused on films grown at controlled substrate temperatures during sputtering. When annealing was performed, the samples were kept under vacuum, heated with the built-in substrate heater, held for the selected duration, and then cooled in the chamber before venting.

4.5 MgO-Based Template Preparation and CMS Growth

After establishing the baseline CMS growth process on Si/SiO_2, the project moved toward MgO substrates and MgO buffer layers. AFM was used as the main feedback tool for evaluating surface roughness after each processing step.

MgO substrates were annealed at 940°C for 1 h in vacuum. In the optimized in-situ process, the substrate was cooled to 400°C after the anneal and a 10 nm MgO buffer layer was deposited at an Ar pressure of approximately 1.4 mTorr without breaking vacuum. This sequence was designed to minimize surface contamination and prepare a smooth MgO-based template for subsequent CMS growth.

MNC072 was deposited at room temperature on a bare MgO substrate at an Ar pressure of approximately 2.03 mTorr and subsequently annealed at 600°C for 15 min. MNC074 was deposited at 550°C on a MgO substrate with the in-situ 10 nm MgO buffer and subsequently annealed at 550°C for 15 min. AFM characterization of MNC074 showed a substantially rougher surface than MNC072, and further

characterization is pending recipe optimization.

Chapter 5

Results and Discussion

This chapter presents the experimental results in the order in which the project developed. Each step was motivated by the outcome of the previous one: the composition-control problem identified in the early target studies led to baseline growth using the commercial CMS target, and the limitations of Si/SiO_2 as a device template then motivated the transition to MgO substrates and MgO buffer layers. The discussion therefore follows the materials path from sputtered CMS films toward CMS/MgO/CMS MTJ preparation.

5.1 Baseline CMS Films on Si/SiO_2

After the exploratory composite-target work described in Chapter 4, the commercial Co_2MnSi bulk target was used as the main route for systematic CMS film growth on Si/SiO_2 substrates. This section characterizes the resulting films in terms of composition, crystal structure, magnetic properties, in-plane anisotropy, and electrical transport.

5.1.1 Film Composition from XPS

The earliest composite-target film gave an XPS-derived composition of Co:Mn:Si = 44.25:18.40:37.36 at.%, which is strongly Mn deficient and Si rich relative to the ideal Co_2MnSi stoichiometry. Because this route did not produce a composition close enough to the desired 2:1:1 ratio, it was not used as the main growth route for the later systematic study.

After the commercial CMS bulk target became available, films grown under both DC and RF sputtering conditions were analyzed by XPS. The film deposited at DC 100 W gave Co:Mn:Si = 43.69:12.04:44.26 at.%, while the film deposited at RF 60 W gave Co:Mn:Si = 40.93:14.54:44.52 at.%. These values are summarized in Table 5.1 and compared with the ideal Co_2MnSi composition.

Table 5.1: XPS-derived compositions of representative CMS films grown from the composite target and the commercial bulk target.

Film / growth route	Co (at.%)	Mn (at.%)	Si (at.%)
Composite target film	44.25	18.40	37.36
Bulk target, DC 100 W	43.69	12.04	44.26
Bulk target, RF 60 W	40.93	14.54	44.52
Ideal Co_2MnSi	50.00	25.00	25.00

The most important trend is the systematic Mn deficiency. This deficiency appears both in the composite-target film and in the films grown from the commercial bulk target, indicating that it is not simply a consequence of one particular target geometry. Several factors may contribute to this behavior, including different sputtering yields of Co, Mn, and Si, preferential oxidation of Mn, and possible resputtering or reduced incorporation of Mn during growth. Since Mn-related disorder and Co-Mn antisites are known to affect the minority spin gap in Co_2MnSi, this composition trend is directly relevant to the magnetic and spintronic properties of the films.

The apparent Si enrichment should be interpreted with caution. XPS is a surface-sensitive technique, and the measured Si signal may include contributions from surface oxides, interfacial SiO_2, or the Si/SiO_2 substrate, especially for thin films. In addition, the Ar^+ sputter-cleaning or etching step used before XPS analysis can modify the near-surface composition. Preferential sputtering or ion-beam-induced changes may reduce the apparent Mn signal or alter the chemical state of Mn, making the absolute Mn concentration extracted from XPS less reliable than the trend itself. Therefore, the XPS results should not be read as a direct measurement of the bulk CMS stoichiometry alone. Instead, they are best interpreted as evidence for a reproducible compositional trend, which should be checked by complementary measurements such as EDS, depth-dependent XPS, or cross-sectional TEM/EDS. Nevertheless, the persistent combination of low apparent Mn content and high apparent Si content shows that composition control remains a central challenge in the present sputtering process.

5.1.2 Crystal Structure from XRD

X-ray diffraction was used to determine whether the bulk-target films grown on Si/SiO_2 formed a crystalline CMS phase. Figure 5.1 shows a representative XRD pattern from MNC053. The observed peaks include CMS-related reflections indexed as (200), (220), and (400).

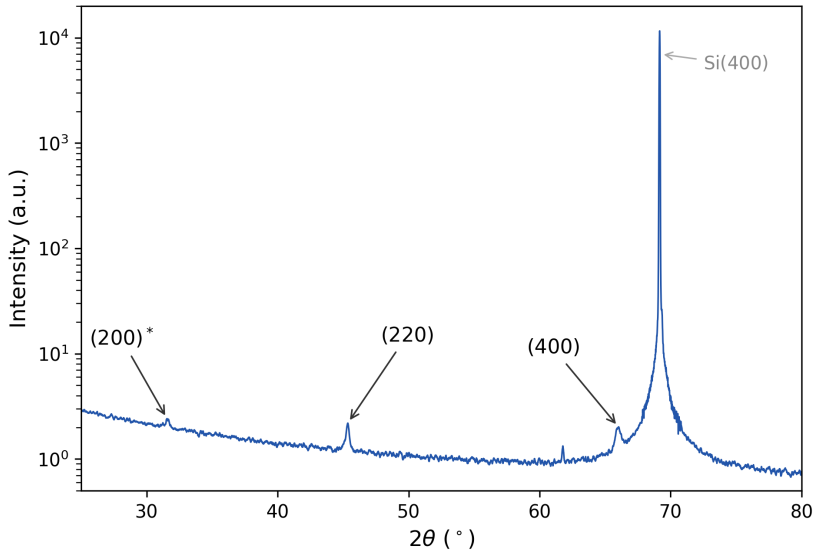

Figure 5.1: Representative XRD pattern of a bulk-target CMS film on Si/SiO_2, with CMS-related (200), (220), and (400) reflections labeled.

The (220) and (400) reflections are fundamental CMS reflections present in all ordering states and confirm the formation of a crystalline CMS-related phase. The (200) reflection, which is absent in the fully disordered A2 structure but allowed in both B2 and $L2_1$ phases, indicates that some degree of chemical ordering beyond A2 has been achieved. A (111) superlattice reflection, which would be the clearest signature of full $L2_1$ order, is not resolved in the present data. This should be interpreted with care: the (111) structure factor in CMS is intrinsically small relative to (220), and in polycrystalline thin films the combination of random grain orientation and limited film thickness makes the (111) peak difficult to detect even when some $L2_1$ order is present. The absence of a clear (111) peak therefore means that full $L2_1$ order cannot be confirmed, rather than that it is definitively absent.

More broadly, achieving well-developed $L2_1$ order on Si/SiO_2 is inherently difficult. The amorphous SiO_2 surface provides no crystallographic template for epitaxial CMS growth, so the film grows as a polycrystal with randomly oriented grains. Establishing long-range chemical order in this environment requires sufficient atomic mobility at each sublattice site, a condition that is considerably harder to satisfy than in films

grown on a lattice-matched crystalline substrate such as MgO(001).[5, 3] The XRD result is therefore consistent with a B2-type or partially ordered structure, and the transition to MgO substrates in Section 5.2 is motivated in part by the expectation that a crystalline template will promote better ordering.

5.1.3 Magnetic Properties from VSM

Room-temperature VSM measurements were performed on four bulk-target films deposited at 480, 500, 520, and 540°C. The extracted saturation magnetizations and coercive fields are listed in Table 5.2, and the corresponding hysteresis loops are shown in Fig. 5.2.

Table 5.2: VSM results for the bulk-target Si/SiO_2 temperature series.

Sample	T_{dep} (°C)	Thickness (nm)	M_s (emu/cm^3)	H_c (Oe)
MNC059	480	67.08	854	9.32–9.96
MNC056	500	66.87	839	4.88–6.49
MNC057	520	67.28	791	7.29–7.51
MNC060	540	67.08	848	8.76–9.35

All films show soft in-plane ferromagnetism with small coercive fields and a strongly suppressed out-of-plane response, consistent with thin-film shape anisotropy. The saturation magnetization ranges from 791 to 854 emu/cm^3 across the 480–540°C window, with no systematic dependence on deposition temperature, as summarized in Fig. 5.3. This indicates that within the explored range, M_s is not strongly sensitive to deposition temperature and is instead governed primarily by the compositional and structural limitations identified in the preceding sections. All values fall noticeably below the $\sim 10^3$ emu/cm^3 expected for fully ordered $L2_1$ CMS,[8, 12] consistent with the Mn deficiency and partial B2-type ordering established by XPS and XRD.

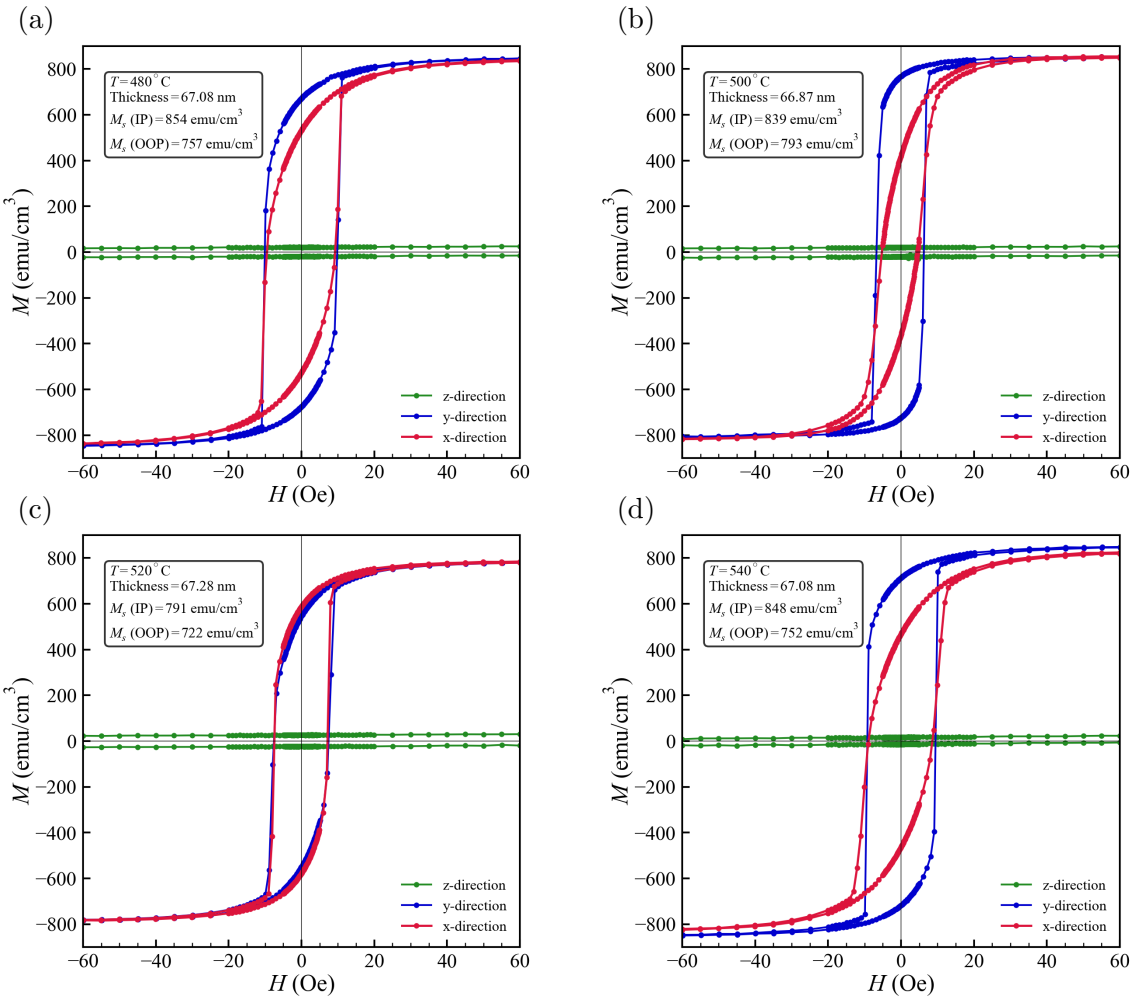

Figure 5.2: VSM hysteresis loops for bulk-target CMS on Si/SiO_2: (a) MNC059, 480°C; (b) MNC056, 500°C; (c) MNC057, 520°C; (d) MNC060, 540°C.

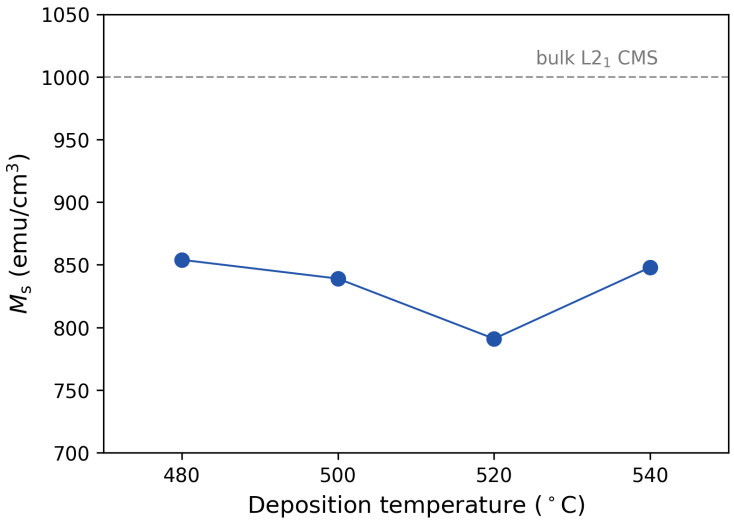

Figure 5.3: M_s as a function of deposition temperature for the Si/SiO_2 bulk-target series. The dashed line indicates the value expected for fully ordered $L2_1$ CMS.

5.1.4 In-Plane Magnetic Anisotropy

Angle-dependent VSM measurements were performed on MNC056 to identify the in-plane easy- and hard-axis-like directions. Figure 5.4 shows two representative loops measured at different azimuthal angles. One direction exhibits a squarer switching loop and larger remanence, consistent with easy-axis-like behavior. The other direction shows a more gradual approach to saturation, consistent with hard-axis-like behavior.

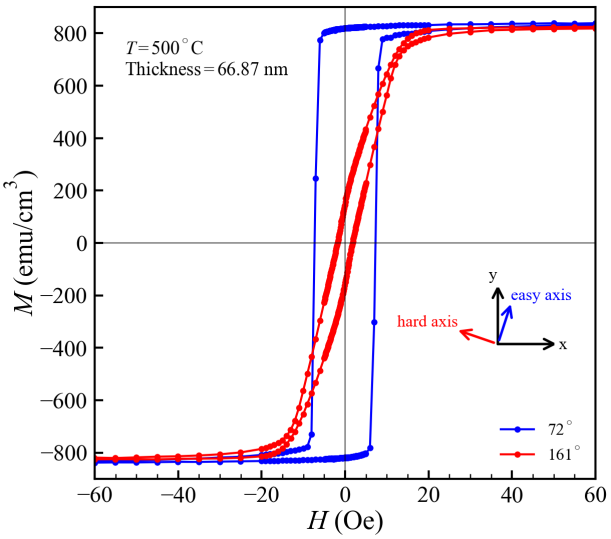

Figure 5.4: Angle-dependent VSM loops for MNC056 grown on Si/SiO_2 at $T_{dep} = 500°C$. The loop at approximately 72° shows easy-axis-like behavior, while the loop at approximately 161° shows hard-axis-like behavior.

The presence of a well-defined in-plane anisotropy is relevant for future MTJ switching. In a CMS/MgO/CMS junction, the two CMS electrodes should ideally be oriented along the same in-plane easy axis, while their different coercive fields allow field-controlled selection of parallel and antiparallel magnetic states. A complete discussion of this device concept is given in Chapter 6.

5.1.5 Electrical Resistivity

Four-probe measurements were used to determine the room-temperature resistivity of the CMS films grown on Si/SiO_2. The measured values fall in the range of 58–77 $\mu\Omega$·cm, confirming metallic transport in the bulk-target CMS films. These values are consistent with the range reported for sputtered CMS thin films in the literature.[5, 3]

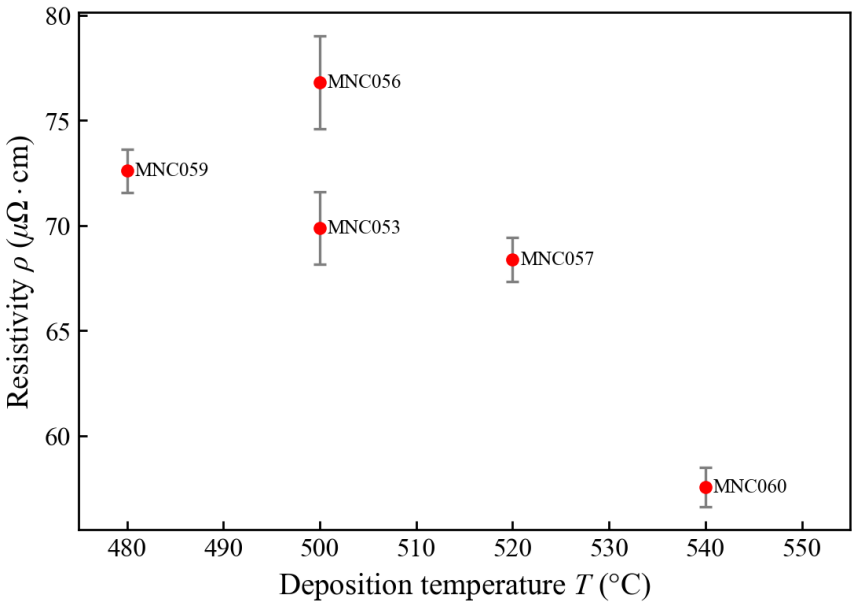

Figure 5.5: Room-temperature resistivity of CMS films grown on Si/SiO_2 as a function of deposition temperature. The values fall in the range of 58–77 $\mu\Omega$·cm, confirming metallic transport.

The slight decrease in resistivity at higher deposition temperature may be consistent with reduced structural disorder or improved grain connectivity, although a more detailed microstructural analysis would be needed to separate these effects quantitatively. Taken together with the XRD and VSM results, the transport measurements show that the commercial bulk target can reproducibly produce CMS films on Si/SiO_2 that are crystalline, ferromagnetic, and metallic.

5.1.6 Summary of Si/SiO_2 Baseline Results

The Si/SiO_2 bulk-target study establishes a reproducible baseline for sputtered CMS film growth. Across the 480–540°C deposition-temperature range, the films are crystalline, ferromagnetically ordered, and electrically metallic. At the same time, the saturation magnetization remains below the value expected for fully ordered $L2_1$ CMS, consistent with the systematic Mn deficiency and partial B2-type ordering identified by XPS and XRD. Beyond the compositional and structural limitations, the amor-

phous SiO_2 surface does not provide a crystallographic template that could support oriented, epitaxially textured CMS growth or a well-defined MgO tunnel barrier. These results define the starting point for the MgO-based work described in the following section, where the focus shifts from establishing whether CMS can be grown at all to controlling the interface quality needed for tunnel junction fabrication.

5.2 Interface Engineering on MgO Substrates

The next part of the project focused on MgO substrates and MgO buffer layers. The purpose was to optimize the surface roughness of the MgO-based template and then evaluate whether CMS could be grown on this template while preserving a smooth surface suitable for future MgO tunnel-barrier deposition.

5.2.1 MgO Buffer Layer Roughness Optimization

Surface roughness is especially important for MTJ fabrication because the MgO tunnel barrier is only 2–3 nm thick. Roughness in the bottom template causes lateral thickness fluctuations in the barrier, which can produce pinholes, nonuniform current distribution, and suppressed coherent tunneling. AFM was used at each stage of the MgO preparation process to monitor surface quality.

After annealing the MgO substrate at 940°C for 1 h, the sample was removed from vacuum for an initial AFM check. The measured RMS roughness of the bare annealed substrate was approximately 0.18 nm, confirming that the substrate surface remained smooth after the high-temperature anneal. The sample was then re-loaded and a 10 nm MgO buffer layer was deposited. The buffer surface (MNC071) showed an RMS roughness of 1.754 nm, substantially rougher than the substrate itself. This result indicated that re-exposure to air between the anneal and the buffer deposition introduced surface contamination that degraded the growing buffer film.

Based on this observation, the process was revised so that the substrate anneal and MgO buffer deposition were carried out in the same vacuum cycle without breaking vacuum. In this in-situ route, the substrate was annealed at 940°C, cooled to 400°C, and the 10 nm MgO buffer was deposited immediately. The resulting buffer surface (MNC073) had a raw RMS roughness of 0.935 nm, reduced to 0.057 nm after polynomial background correction to remove long-range substrate bow and scanner drift. This corrected value is comparable to the as-received substrate roughness and is appropriate for growing a uniform 2–3 nm MgO tunnel barrier.

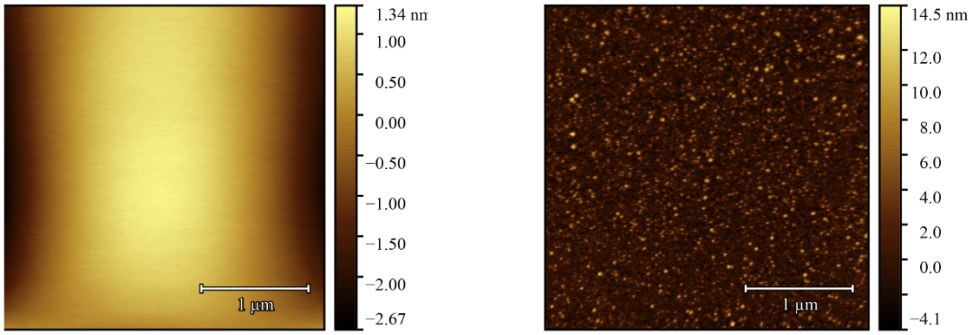

Figure 5.6: AFM topography of MgO buffer layers deposited after breaking vacuum (MNC071, RMS = 1.754 nm) and in-situ without vacuum break (MNC073, RMS = 0.057 nm after background correction).

The MgO deposition rate was also calibrated separately using XRR to support future tunnel-barrier growth; the details and resulting deposition parameters are discussed in the context of the MTJ stack design in Section 6.1. This finding directly shaped the subsequent CMS deposition strategy. MNC072, which was grown before this protocol was established, was deposited directly on a bare MgO substrate without a buffer layer. MNC074, prepared after MNC073, was the first CMS sample to incorporate the in-situ MgO buffer, and also explored the effect of elevated deposition temperature. The properties of both samples are discussed in the following section.

5.2.2 CMS on MgO: Morphology, Structure, and Magnetism

Two CMS samples were grown on MgO-based templates to evaluate film quality and begin exploring the effects of deposition conditions. MNC072 was deposited directly on a bare MgO substrate before the buffer protocol was established, while MNC074 incorporated the in-situ MgO buffer developed in the preceding section and used elevated-temperature deposition. Their processing conditions are summarized in Table 5.3.

Table 5.3: CMS-on-MgO samples and processing conditions.

Parameter	MNC072	MNC074
MgO buffer	None (direct on substrate)	10 nm in-situ
CMS thickness	30 nm	20 nm
Deposition temperature	Room temperature	550°C
Annealing temperature	600°C	550°C
Annealing time	15 min	15 min

Surface morphology (AFM)

AFM of MNC072 after CMS deposition and annealing gave an RMS roughness of 0.178 nm, showing that CMS growth on MgO and subsequent 600°C annealing preserved the smooth substrate surface. This result is encouraging from a device perspective: a CMS surface at this roughness level is compatible with the deposition of a uniform 2–3 nm MgO tunnel barrier.

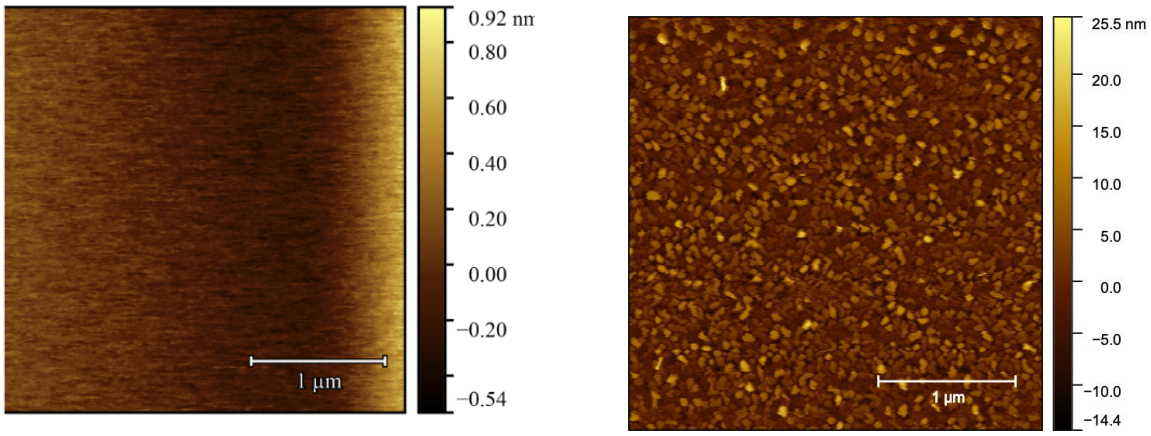

Figure 5.7: AFM surface topography of MNC072 (left, RT deposition, $R_q = 0.178$ nm) and MNC074 (right, 550°C deposition, granular surface).

In contrast, MNC074, which was deposited at 550°C on the in-situ MgO buffer, showed a substantially rougher surface. The elevated deposition temperature under the current sputtering conditions appears to promote island growth rather than smooth layer-by-layer growth, resulting in a granular surface morphology that is not yet suitable for tunnel barrier deposition. This indicates that the deposition parameters for elevated-temperature CMS growth on MgO require further optimization before the structural and magnetic properties of such films can be meaningfully characterized.

Thickness and interface quality (XRR)

XRR of MNC072 confirms the CMS film thickness and provides a measure of interface quality. The Kiessig fringes visible in Fig. 5.8 persist to $2\theta \approx 5°$, indicating a well-defined CMS/MgO interface. A fit to the fringe spacing yields a CMS thickness of 28.65 ± 2.96 nm, consistent with the nominal 30 nm deposition target within the measurement uncertainty.

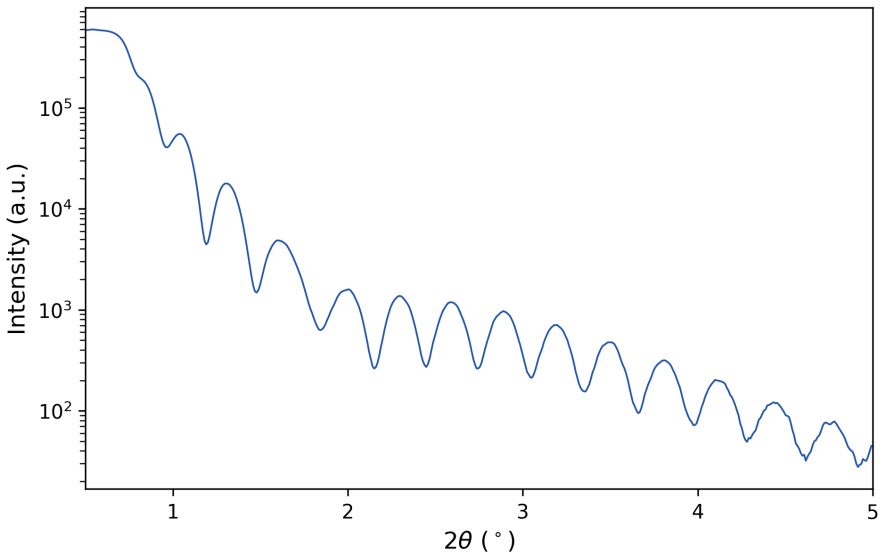

Figure 5.8: XRR pattern of MNC072 (30 nm CMS on MgO). Kiessig fringes are visible to $2\theta \approx 5°$. The fitted CMS thickness is 28.65 ± 2.96 nm.

Crystal structure (XRD)

XRD characterization of MNC072 and MNC074 is not yet complete. As a structural reference for what CMS growth on MgO can achieve, Fig. 5.9 shows XRD patterns from the literature for CMS films grown on MgO(001) at different deposition temperatures and annealed at 550°C.[24] The (002) and (004) CMS reflections, which correspond to the (001) preferred orientation expected for CMS on MgO, become stronger and better defined with increasing deposition temperature. The appearance of the (111) superlattice reflection in the ϕ-scan confirms $L2_1$ ordering in the sample deposited at 550°C. These results establish the structural benchmark that the present MgO-based growth is working toward: well-defined CMS reflections, (001) texture, and partial or full $L2_1$ ordering. Once the surface morphology of elevated-temperature CMS deposition on MgO is improved, XRD will be used to evaluate whether similar ordering can be achieved in our system.

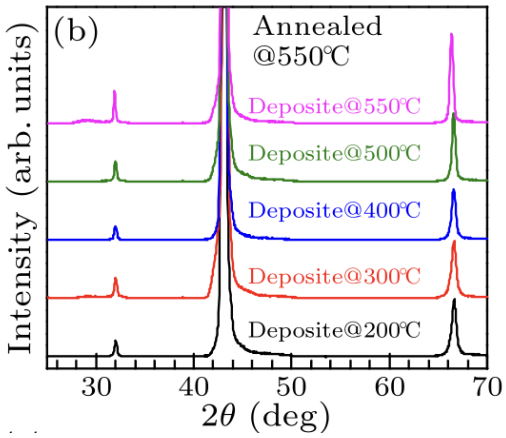

Figure 5.9: XRD patterns of CMS films on MgO(001) at different deposition temperatures, annealed at 550°C (adapted from Ref. [24]).

Magnetic properties (VSM)

The two CMS-on-MgO samples show strikingly different magnetic behavior, reflecting the different deposition strategies used. MNC072, deposited at room temperature without a buffer layer and annealed at 600°C, gives $M_s = 741$ emu/cm^3. Its angle-dependent VSM loops at 0°, 30°, 60°, and 90° are nearly identical in shape, with coercive fields of 65–73 Oe across all angles and no resolvable in-plane anisotropy (Fig. 5.10(a)). This is consistent with room-temperature deposition on a bare MgO substrate: without sufficient adatom mobility during growth, the epitaxial registry between CMS and MgO is not well established, and no magnetocrystalline anisotropy develops even after the 600°C post-anneal.

MNC074, deposited at 550°C on the in-situ MgO buffer and annealed at 550°C, shows qualitatively different behavior. Its saturation magnetization of $M_s = 791$ emu/cm^3 is higher than MNC072, and its angle-dependent loops show a clear dependence on azimuthal angle, with coercive fields ranging from 135 Oe at 30° to 235 Oe at 0° (Fig. 5.10(b)). The minimum in H_c near 30° and the maximum near 0° and 90° are consistent with fourfold in-plane magnetic anisotropy arising from the cubic symmetry of the CMS/MgO epitaxial system, in good agreement with results reported

by Qiao *et al.* for CMS deposited at 550°C on MgO.[24] The appearance of this anisotropy confirms that elevated-temperature deposition promotes sufficient epitaxial alignment between CMS and MgO to establish a magnetocrystalline easy axis, even in a sputtered film. The M_s of MNC074 is also comparable to the Si/SiO_2 baseline films ($\sim$800 emu/cm^3), suggesting that the combination of the in-situ buffer and elevated deposition temperature does not sacrifice magnetic quality despite the rougher surface.

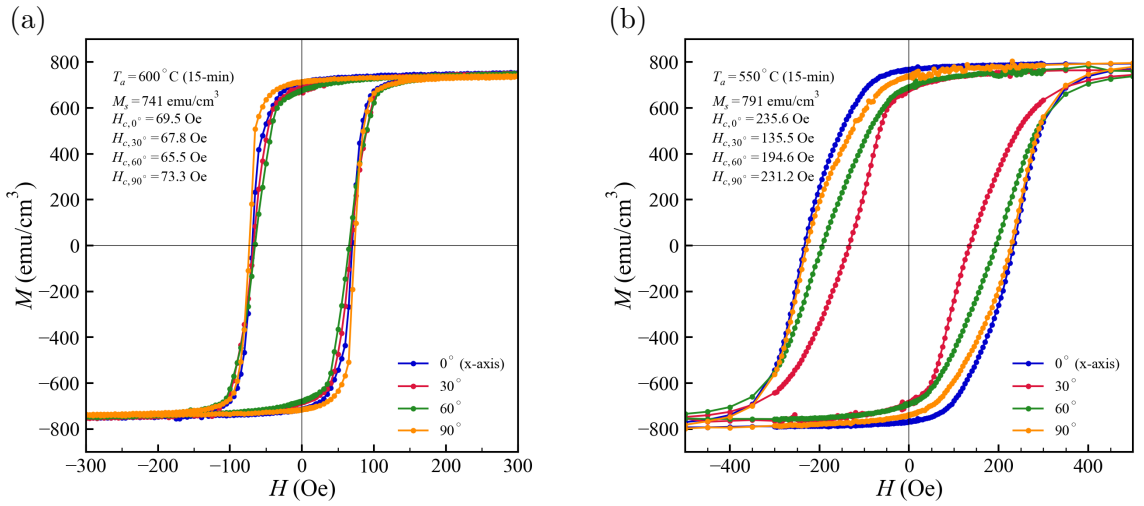

Figure 5.10: Angle-dependent VSM loops for (a) MNC072 (RT deposition, T_a = 600°C, M_s = 741 emu/cm^3) and (b) MNC074 (550°C deposition, in-situ buffer, T_a = 550°C, M_s = 791 emu/cm^3).

5.2.3 Summary of MgO-Based Interface Engineering

The MgO-based results establish the current state of CMS/MgO heterostructure development in our laboratory on two fronts. On the morphology side, the in-situ buffer protocol reduces local MgO template roughness to 0.057 nm, and CMS deposited at room temperature on a bare MgO substrate preserves a smooth surface of 0.178 nm with a well-defined CMS/MgO interface confirmed by XRR. These values are appropriate for uniform MgO tunnel barrier growth.

On the magnetic side, the two CMS-on-MgO samples tell a more nuanced story. MNC072 shows M_s = 741 emu/cm^3 but no resolvable in-plane anisotropy, while

MNC074 achieves $M_s = 791$ emu/cm^3 and clear fourfold in-plane anisotropy consistent with epitaxial CMS/MgO alignment, at the cost of a rougher surface. Together, these two samples define the central trade-off: surface smoothness favors lower deposition temperature, while magnetic ordering and anisotropy favor higher temperature. Resolving this trade-off through systematic optimization of deposition conditions is the immediate next step before the MgO-based CMS films are ready for MTJ stack fabrication, as discussed in Chapter 6.

Chapter 6

Toward CMS/MgO/CMS Magnetic Tunnel Junctions

Chapter 5 established two prerequisites for moving toward CMS/MgO/CMS magnetic tunnel junctions: a reproducible ferromagnetic CMS electrode process and a smooth MgO-based template prepared by the in-situ buffer protocol. The Si/SiO_2 baseline films confirmed that sputtered CMS can be crystalline, ferromagnetic, and metallic, while the MgO-based experiments showed that the template roughness can be reduced to the level required for tunnel-barrier growth. Building on those results, this chapter defines the proposed MTJ stack architecture, switching strategy, fabrication sequence, and the remaining gap between the current film quality and the requirements for high TMR.

6.1 MTJ Stack Architecture

The proposed MTJ stack is built on an MgO(001) substrate and consists, from bottom to top, of a 10 nm MgO buffer layer, a CMS bottom electrode, a 2–3 nm MgO tunnel barrier, a CMS top electrode, and a metallic capping layer (∼5 nm, Ta, Ru, or Cr, to be determined). The exact CMS electrode thicknesses are still under investigation,

as the systematic thickness and deposition-temperature optimization described in Section 5.2.2 is ongoing. The thickness asymmetry between the two electrodes is a key design parameter because it determines the coercive field difference needed for field-controlled P/AP switching, and will be fixed once the single-layer CMS optimization on MgO substrates is complete.

The MgO(001) substrate provides the crystalline template for the MTJ stack. MgO has a cubic lattice parameter of approximately 4.212 Å, and the commonly used 45°-rotated epitaxial relationship between CMS and MgO gives a lattice mismatch of about 3.7%. This mismatch is small enough to make MgO a natural substrate and barrier material for CMS-based epitaxial MTJs, as shown in the high-TMR CMS/MgO/CMS literature.[13, 9]

The 10 nm MgO buffer layer is deposited in situ at 400°C using the protocol developed in Section 5.2.1. Its purpose is to provide a clean and smooth nucleation surface for CMS growth. The AFM results in Chapter 5 show that this process produces a locally smooth MgO template with $R_{\mathrm{q}} \approx 0.06$ nm after background correction, which is important because the MgO tunnel barrier will be only a few nanometers thick.

The CMS bottom electrode serves as the main magnetic electrode of the MTJ. It will be deposited by RF sputtering using conditions developed in the MgO-substrate optimization series. Its thickness will be chosen to be substantially larger than that of the top electrode, so that its larger magnetic volume produces a higher coercive field and ensures that the two electrodes switch at well-separated field values. The deposition temperature and annealing conditions will follow the optimized recipe established from the MNC072 and MNC074 series, targeting partial or full $L2_1$ ordering and M_{s} approaching 10^3 emu/cm^3.

The MgO tunnel barrier is designed to be 2–3 nm thick. It will be deposited by RF sputtering at 70 W under an Ar pressure of approximately 1.34 mTorr, using the MgO deposition rate calibrated by XRR at 0.21 Å/s. The 2–3 nm range balances

two competing requirements: the barrier must be thick enough to avoid pinholes and direct metallic shorts, but thin enough to keep the junction resistance within a measurable tunneling range. The barrier will be deposited at room temperature to preserve the CMS/MgO interface and minimize intermixing at the CMS surface.

The CMS top electrode will be deposited under the same sputtering conditions as the bottom electrode. Its thickness will be chosen to be substantially thinner than the bottom electrode so that its smaller magnetic volume gives a lower coercive field, enabling it to switch before the bottom electrode during a field sweep. The precise thickness ratio between the two electrodes will be determined from single-layer VSM measurements once the MgO-substrate optimization is complete.

The stack is completed by a metallic capping layer (Ta, Ru, or Cr, to be determined) with a thickness of approximately 5 nm. This layer will be deposited in situ immediately after the top CMS electrode without breaking vacuum. Its role is to prevent oxidation of the thin CMS top electrode during air exposure and to provide a low-resistance electrical contact for the lithographically defined top electrode. The single-layer CMS samples discussed in Chapter 5, including MNC072 and MNC074, were grown without a capping layer because they were intended for structural, surface, and magnetic characterization only; the full MTJ stack will include this protective cap.

6.2 Switching Strategy: Coercive Field Asymmetry

To measure TMR, the two ferromagnetic electrodes must be switched between parallel and antiparallel configurations. In conventional MTJs this is often achieved by using exchange bias to pin one electrode while allowing the other to switch freely. In the present first-generation CMS/MgO/CMS design, no exchange-bias layer is in-

cluded. Instead, the device relies on a coercive-field difference between the two CMS electrodes.

The intended coercive-field asymmetry comes from the thickness difference between the two CMS electrodes. The bottom CMS electrode is designed to be substantially thicker than the top electrode. A larger magnetic volume generally produces a larger energy barrier against magnetization reversal and therefore a higher switching field. The in-plane coercive fields measured for the Si/SiO_2 CMS films in Chapter 5 were approximately 5–10 Oe for films around 67 nm thick, providing a rough reference scale for soft CMS films. The actual coercive fields of the bottom and top CMS layers on MgO must be determined from VSM measurements of single-layer MgO-substrate samples once the thickness optimization is complete, including MNC072, MNC074, and subsequent samples in the ongoing series.

The field-sweep protocol follows directly from this asymmetry. Starting from positive saturation, both CMS electrodes are aligned in the same direction, so the junction is in the parallel state and has the lower resistance R_{P}. As the magnetic field is swept toward negative values, the thinner top electrode should switch first, producing an antiparallel state with the higher resistance R_{AP}. With further increase of the negative field, the thicker bottom electrode switches, returning the junction to a parallel state with low resistance. The resulting resistance versus field curve should show a two-step signature: a step up when the top electrode switches and a step down when the bottom electrode switches.

The fourfold in-plane anisotropy observed in MNC074 confirms that a well-defined easy axis can be established in CMS films on MgO under elevated-temperature deposition conditions. For the MTJ measurement, the field sweep should be applied along the easy axis direction ($\sim 30^\circ$ from the x-axis in MNC074) to obtain clean and reproducible switching. Further optimization of the deposition conditions to reduce surface roughness while preserving the anisotropy will determine the final electrode

recipe.

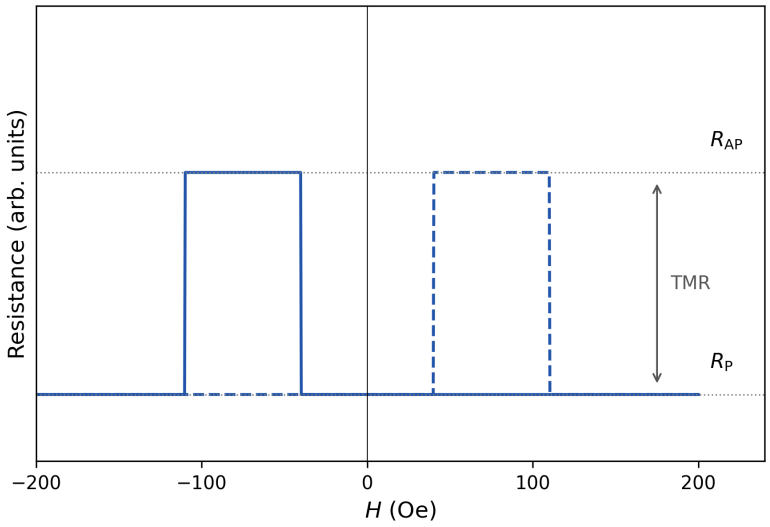

Figure 6.1: Schematic R vs H curve for a CMS/MgO/CMS MTJ showing the parallel (R_{P}) and antiparallel (R_{AP}) resistance states.

6.3 Junction Resistance and Mask Design

Using the Julliere model and the MgO barrier parameters selected for this design, the expected junction resistance falls within a measurable range for standard four-probe dc transport and PPMS measurements. For a 2–3 nm MgO barrier and area-resistance products consistent with RF-sputtered MgO barriers, the estimated antiparallel resistance R_{AP} for junction areas ranging from approximately 900 μm^2 for a 30 μm diameter circle to approximately 6360 μm^2 for a 90 μm diameter circle is about 10–85 kΩ. This range is high enough to avoid being dominated by lead and contact resistance, but low enough to be measured reliably with standard dc instrumentation. These estimates guided the choice of junction dimensions in the mask design.

The MTJ mask has been designed and finalized. The junction geometries include circular junctions with diameters from 30 to 90 μm, elliptical junctions with fixed area of 2200 μm^2, and elliptical junctions with fixed width of 30 μm. The layout is compatible with both wire-bonding and probe-station measurements, and each unit

cell fits on a 5×5 mm chip. This geometry allows the same material stack to be tested across different junction areas and contact configurations.

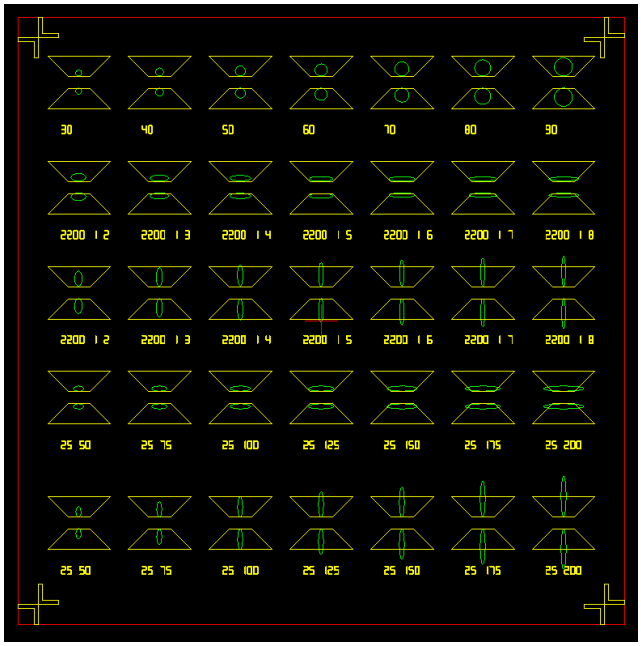

Figure 6.2: MTJ mask layout for 5×5 mm chips, including circular (D = 30–90 μm) and elliptical junction geometries.

6.4 Fabrication Sequence

The first-generation CMS/MgO/CMS MTJ devices will be fabricated using the following process sequence.

1. **Full stack deposition.** The complete layer sequence defined in Section 6.1 is deposited in a single vacuum cycle without breaking vacuum between layers. Deposition conditions for each layer follow those described in Section 6.1.

2. **Pillar definition by photolithography and ion milling.** A positive photoresist pillar mask is patterned by photolithography to define the junction area. Ar ion milling is then used to etch through the metallic cap, the top CMS electrode, and the MgO barrier, stopping on the bottom CMS layer. The etch endpoint is monitored by secondary ion signal.

3. **Sidewall insulation.** A second lithography step opens a window around the etched pillar. Approximately 50 nm SiO_2 is deposited by RF sputtering, followed by lift-off to electrically isolate the top electrode from the bottom CMS layer.

4. **Top contact metallization.** A third lithography step defines the top electrode pad geometry. Cr (5 nm) / Au (100 nm) is deposited by dc sputtering and lifted off to form low-resistance contact pads compatible with both wire bonding and probe-station measurement.

Following device fabrication, four-terminal dc transport measurements will be performed in the PPMS or probe station 3. The magnetic field will be swept between ± 500 Oe along the in-plane easy axis, and the junction resistance $R(H)$ will be recorded at both 300 K and 4.2 K to characterize the TMR ratio and its temperature dependence.

6.5 Gap Analysis: Current Films vs High-TMR Requirements

The present results show that the project has reached the point where a CMS/MgO/CMS stack can be designed realistically, but they also clarify why a large TMR ratio should not yet be assumed. The most important remaining issue is the CMS composition. Across all routes tested so far, including the composite Co/Mn/Si target and the commercial bulk CMS target under both DC and RF sputtering, the films remain Mn deficient relative to the ideal Co:Mn:Si = 2:1:1 stoichiometry. The measured Mn content falls in the range of approximately 12–18 at.%, well below the ideal 25 at.%. This is a serious limitation because the CMS/MgO/CMS literature shows that the electrode composition directly affects TMR. In particular, Ishikawa *et al.* showed

that Mn-rich $Co_2Mn_\alpha Si$ electrodes can produce much higher TMR than nearly stoichiometric electrodes, which was attributed to the suppression of Co-Mn antisites and the reduction of minority-spin gap states.[14] In the present films, the opposite tendency appears: Mn is deficient rather than enriched. Therefore, composition engineering is the highest-priority problem before the present CMS films can be expected to approach the half-metallic behavior needed for high TMR.

The reduced saturation magnetization and incomplete ordering are likely connected to this composition problem. The Si/SiO_2 baseline films show clear CMS-related XRD reflections and a chemically sensitive (200) peak, indicating crystalline CMS with partial chemical ordering, but no clear (111) superlattice peak has yet been established. This means that the films should be regarded as partially ordered, rather than fully $L2_1$ ordered. Their measured saturation magnetization, approximately 750–800 emu/cm^3, is also below the value expected for highly ordered CMS, which is close to 10^3 emu/cm^3.[1, 8] These two observations are consistent with the same underlying limitation: off-stoichiometry and antisite disorder reduce both the magnetic moment and the spin polarization. XRD measurements on MNC072 and MNC074 are currently in progress and will determine whether the MgO substrate promotes better crystallographic ordering than Si/SiO_2.

The interface morphology problem is in a better position. The in-situ MgO buffer protocol developed in this work reduced the local roughness of the MgO-based template to about 0.06 nm after background correction, and CMS grown on this template preserved a smooth surface with $R_q = 0.178$ nm. MNC074 further shows that elevated-temperature deposition on the in-situ buffer can raise M_s to 791 emu/cm^3 with fourfold in-plane anisotropy, though at the cost of increased surface roughness. This suggests that the topographic requirement for depositing a continuous 2–3 nm MgO tunnel barrier can be met. However, smooth morphology does not by itself guarantee a high-quality tunneling interface. The CMS/MgO interface must also be

chemically sharp and electronically clean. Tunneling spectroscopy studies have shown that minority-spin interface states can strongly influence spin-dependent tunneling in CMS/MgO/CMS junctions, even when the bulk electrode is close to half metallic.[10] For the present sputtered films, the key unresolved interface questions are whether Mn oxidizes during MgO barrier deposition or annealing, whether the CMS/MgO interface remains abrupt, and whether the MgO barrier develops the crystallinity needed for symmetry-filtered tunneling.

Taken together, the results suggest that the project is now limited less by basic film continuity or template roughness and more by the electronic quality of the CMS electrodes and CMS/MgO interface. The in-situ MgO buffer process has created a viable platform for building the first MTJ stack, but the expected TMR will depend on whether future growth can raise the Mn content, improve $L2_1$ ordering, and preserve a chemically clean MgO barrier interface. These are the main materials gaps between the present films and the epitaxial CMS/MgO/CMS MTJs that have produced very large TMR values in the literature.[13, 9, 15]

6.6 Future Experiments

The next experiments should focus on making the CMS electrode on MgO closer to the half-metallic limit before moving too aggressively into full device fabrication. MNC072 and MNC074 represent the first two points in this process: MNC072 tests room-temperature CMS deposition followed by high-temperature annealing, while MNC074 begins to explore elevated-temperature deposition and a thinner CMS layer. A more systematic series should vary CMS thickness over a broad range, for example 10–60 nm, while also varying deposition and annealing temperature between roughly 400 and 700°C. The most important signs of success would be the appearance of the (111) superlattice peak in XRD, narrower CMS diffraction peaks, and an increase

of M_s toward or above 900 emu/cm^3. Those results would indicate that the MgO substrate is not only producing a smooth surface, but also helping the CMS film approach stronger $L2_1$ order. The optimized thickness and deposition conditions emerging from this series will then determine the final electrode thicknesses used in the MTJ stack.

At the same time, the composition problem needs to be addressed directly. Changing temperature and thickness may improve ordering, but it is unlikely to fully solve the Mn deficiency if the incoming flux is already Mn poor or if Mn is preferentially lost during growth. A practical next step would be to add a supplemental Mn sputter source during CMS deposition and tune the Mn power gradually while keeping the commercial CMS target as the main source. Another route would be to obtain a Mn-rich CMS alloy target, such as $Co_2Mn_{1.3}Si$, or to revisit the composite target with a geometry more strongly biased toward Mn. In each case, the adjustment should be validated by XPS before the process is used for a full MTJ stack. The target is not simply to match the nominal 2:1:1 ratio, but to reach Mn-stoichiometric or slightly Mn-rich CMS, because the literature indicates that this composition range is more favorable for suppressing Co-Mn antisites and improving TMR.[14]

Once the CMS composition and MgO-based growth conditions are improved, the first CMS/MgO/CMS MTJs should be fabricated using the stack architecture and mask design described above. The initial goal should be modest: to observe a clear two-step resistance switching curve that distinguishes the parallel and antiparallel states. Even a moderate TMR ratio would be valuable at this stage because it would confirm that the MgO barrier is continuous, that the two CMS electrodes switch separately, and that the measurement geometry works. After that, temperature-dependent magnetotransport from 4.2 K to 300 K can be used to identify the main spin-depolarization mechanism. If the TMR increases strongly at low temperature, the limitation may be related to thermal spin excitations in a partially half-metallic

electrode. If the temperature dependence is weak, interface disorder or minority-spin interface states are more likely to dominate, as discussed in tunneling studies of epitaxial CMS/MgO/CMS junctions.[10, 15] This comparison will turn the MTJ measurement from a simple device test into a diagnostic tool for the materials problems identified throughout this thesis.

Chapter 7

Conclusions

7.1 Summary of Main Findings

This thesis set out to develop a sputtered Co_2MnSi thin-film process suitable for use as electrodes in CMS/MgO/CMS magnetic tunnel junctions, starting from no established recipe in our laboratory. The work proceeded in three stages, each motivated by the results of the previous one, and the picture that emerges from the combined data is both encouraging and clear about what remains to be done.

The most consistent result across the entire project is that sputtered CMS films are systematically Mn-deficient, regardless of whether a composite Co/Mn/Si target or a commercial bulk CMS alloy target is used. XPS measurements gave Mn contents in the range of 12–18 at.% under all conditions tested, compared to the ideal 25 at.%. This is not a consequence of any single process choice but reflects the combined effect of sputtering yield differences between Co, Mn, and Si, and the tendency of Mn to oxidize and be preferentially lost from the growing film surface. The saturation magnetizations of 750–800 emu/cm^3 and the partial B2-type ordering seen in XRD are both consistent with this compositional shortfall, since off-stoichiometry on the Mn sublattice directly introduces antisite defects that reduce the magnetic moment

and degrade spin polarization.

Within this compositional constraint, a reproducible baseline CMS process was established on Si/SiO_2 substrates. Films deposited in the 480–540°C range at RF 60 W showed clear CMS (220) and (400) reflections, a partial $(200)^*$ ordering signature, soft ferromagnetic hysteresis with coercive fields of 5–10 Oe, metallic resistivities of 58–77 $\mu\Omega$·cm, and a well-defined in-plane easy axis from angle-dependent VSM. These results confirm that sputtered CMS in this system is a viable ferromagnetic electrode material, even if the current composition places it below the half-metallic regime.

Moving to MgO substrates introduced the practical question of how to prepare a buffer layer smooth enough to support a uniform 2–3 nm tunnel barrier. Early process attempts indicated that allowing the substrate to be exposed to air after high-temperature annealing led to unacceptably rough buffer surfaces. Keeping the entire sequence, from substrate annealing through buffer deposition, within a single vacuum cycle resolved this. The resulting in-situ protocol produces a local MgO buffer roughness of 0.057 nm. MNC072 establishes that smooth CMS growth on MgO is possible ($R_q = 0.178$ nm, $M_s = 741$ emu/cm^3) but without in-plane anisotropy. MNC074 demonstrates that the combination of the in-situ MgO buffer and 550°C deposition produces fourfold in-plane magnetic anisotropy and higher M_s (791 emu/cm^3), consistent with improved epitaxial alignment, at the cost of increased surface roughness. These results define the central optimization challenge for the next stage: achieving both smooth morphology and well-defined anisotropy simultaneously.

These results place the project at a well-defined transition point. The interface engineering problem has been addressed, the fabrication sequence and mask design are ready, and the dominant materials challenge is clearly identified: achieving Mn-stoichiometric or slightly Mn-rich CMS electrodes with improved $L2_1$ ordering on MgO. That is the problem the next stage of the project will need to solve.

7.2 Contributions of This Thesis

The most practically transferable contribution of this work is the in-situ MgO buffer deposition protocol. By keeping the substrate anneal and buffer deposition within a continuous vacuum cycle, local surface roughness is reduced to 0.057 nm, which is appropriate for growing a uniform few-nanometer MgO tunnel barrier. Combined with the XRR-calibrated MgO deposition rate of 0.21 Å/s, this protocol can be applied directly to the first full MTJ stack deposition without further modification.

The systematic characterization dataset assembled here also has lasting value for the laboratory independent of the specific samples measured. XPS, XRD, AFM, XRR, VSM, and four-probe resistivity have been applied together to CMS films across two substrate systems and multiple deposition conditions for the first time in this group, providing a quantitative baseline against which all future growth optimization can be evaluated. The XPS composition data in particular, spanning composite-target and bulk-target conditions, establishes that Mn deficiency is a systemic property of the current sputtering process rather than an artifact of any one target design. This considerably narrows the solution space for future composition engineering.

Perhaps more important than any individual result is what this thesis clarifies about where the difficulty actually lies. At the outset it was not obvious whether the main obstacle to a working CMS/MgO/CMS MTJ in this system would be surface roughness, phase formation, electrical continuity, or something else. That question now has a specific answer: the interface morphology is under control, the structural and magnetic baselines are established, and the fabrication path is defined. The gap between the current films and a functional high-TMR device is the composition of the CMS electrodes, and that is a much more tractable problem to hand to the next stage of the project than a general uncertainty about whether the material can be grown at all.

Bibliography

[1] T. Graf, C. Felser, and S. S. P. Parkin, "Simple rules for the understanding of Heusler compounds," *Prog. Solid State Chem.* **39**, 1–50 (2011).

[2] L. J. Singh, *Co_2MnSi Heusler Alloy Thin Films*, Ph.D. thesis, University of Cambridge (2005).

[3] F. J. Yang, W. J. Li, J. H. Li, H. B. Chen, D. G. Liu, X. Q. Chen, and C. P. Yang, "The microstructure and magnetic properties of Co_2MnSi thin films deposited on Si substrate," *J. Alloys Compd.* **723**, 188–191 (2017).

[4] S. Kammerer, A. Thomas, A. Hütten, and G. Reiss, "Room-temperature preparation and magnetic behavior of Co_2MnSi thin films," *J. Appl. Phys.* **93**, 7945–7947 (2003).

[5] K. Kim, S. J. Kwon, and W. T. Kim, "Characterization of Heusler alloy thin film, Cu_2MnAl and Co_2MnSi, deposited by co-sputtering method," *Phys. Status Solidi B* **241**, 1557–1560 (2004).

[6] M. Belmeguenai, H. Tuzcuoglu, M. S. Gabor, F. Zighem, D. Faurie, C. Tiusan, and M. Hehn, "Structural and magnetic properties of Co_2MnSi thin films," *Phys. Status Solidi A* **209**, 1328–1333 (2012).

[7] A. Rajanikanth, Y. K. Takahashi, and K. Hono, "Spin polarization of Co_2MnGe and Co_2MnSi thin films with A2 and $L2_1$ structures," *J. Appl. Phys.* **101**, 023901 (2007).

[8] H. Pandey, P. C. Joshi, R. P. Pant, R. Prasad, S. Auluck, and R. C. Budhani, "Evolution of ferromagnetic and spin-wave resonances with crystalline order in thin films of full-Heusler alloy Co_2MnSi," *J. Appl. Phys.* **111**, 023912 (2012).

[9] H. X. Liu, Y. Honda, T. Taira, K. Matsuda, M. Arita, T. Uemura, and M. Yamamoto, "Giant tunneling magnetoresistance in epitaxial $Co_2MnSi/MgO/Co_2MnSi$ magnetic tunnel junctions by half-metallicity of Co_2MnSi and coherent tunneling," *Appl. Phys. Lett.* **101**, 132418 (2012).

[10] T. Ishikawa, N. Itabashi, T. Taira, K. Matsuda, T. Uemura, and M. Yamamoto, "Critical role of interface states for spin-dependent tunneling in half-metallic Co_2MnSi-based magnetic tunnel junctions investigated by tunneling spectroscopy," *Appl. Phys. Lett.* **94**, 092503 (2009).

[11] M. Jourdan, J. Minár, J. Braun, A. Kronenberg, S. Chadov, B. Balke, A. Gloskovskii, M. Kolbe, H. J. Elmers, G. Schönhense, H. Ebert, C. Felser, and M. Kläui, "Direct observation of half-metallicity in the Heusler compound Co_2MnSi," *Nat. Commun.* **5**, 3974 (2014).

[12] W. H. Wang, X. B. Ren, G. H. Wu, M. Przybylski, J. Barthel, and J. Kirschner, "Magnetic and transport properties of epitaxial Co_2MnSi films," *IEEE Trans. Magn.* **41**, 2805–2807 (2005).

[13] T. Ishikawa, S. Hakamata, K.-i. Matsuda, T. Uemura, and M. Yamamoto, "Fabrication of fully epitaxial $Co_2MnSi/MgO/Co_2MnSi$ magnetic tunnel junctions," *J. Appl. Phys.* **103**, 07A919 (2008).

[14] T. Ishikawa, H. X. Liu, T. Taira, K.-i. Matsuda, T. Uemura, and M. Yamamoto, "Influence of film composition in Co_2MnSi electrodes on tunnel magnetoresistance characteristics of Co_2MnSi/MgO/Co_2MnSi magnetic tunnel junctions," *Appl. Phys. Lett.* **95**, 232512 (2009).

[15] B. Hu, K. Moges, Y. Honda, H.-X. Liu, T. Uemura, M. Yamamoto, J. Inoue, and M. Shirai, "Temperature dependence of spin-dependent tunneling conductance of magnetic tunnel junctions with half-metallic Co_2MnSi electrodes," Phys. Rev. B **94**, 094428 (2016).

[16] A. Wederni *et al.*, "Unveiling strong dependence of geometrical aspect ratio on the magneto-structural properties of Co_2Mn-based microwires," *Preprint*, DOI: 10.20944/preprints202307.1212.v1 (2023).

[17] M. Ohring, *Materials Science of Thin Films*, 2nd ed. (Academic Press, San Diego, 2002).

[18] P. Sigmund, "Theory of sputtering. I. Sputtering yield of amorphous and polycrystalline targets," *Phys. Rev.* **184**, 383–416 (1969).

[19] J. A. Thornton, "Influence of apparatus geometry and deposition conditions on the structure and topography of thick sputtered coatings," *J. Vac. Sci. Technol.* **11**, 666–670 (1974).

[20] B. D. Cullity and S. R. Stock, *Elements of X-Ray Diffraction*, 3rd ed. (Prentice Hall, Upper Saddle River, 2001).

[21] S. Chikazumi, *Physics of Ferromagnetism*, 2nd ed. (Oxford University Press, Oxford, 1997).

[22] D. Briggs and M. P. Seah (eds.), *Practical Surface Analysis*, 2nd ed. (John Wiley & Sons, Chichester, 1990).

[23] J. I. Goldstein, D. E. Newbury, D. C. Joy, C. E. Lyman, P. Echlin, E. Lifshin, L. Sawyer, and J. R. Michael, *Scanning Electron Microscopy and X-Ray Microanalysis*, 3rd ed. (Springer, New York, 2003).

[24] S.-Z. Qiao *et al.*, "Structural and magnetic properties of Co_2MnSi thin film with a low damping constant," *Chin. Phys. Lett.* **32**, 057601 (2015).